

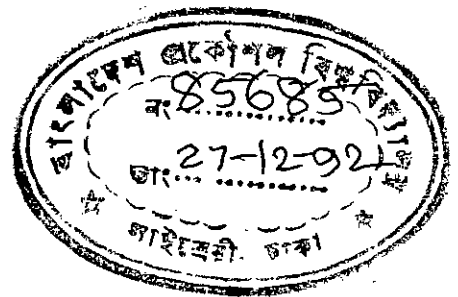
**STUDY OF TURBINE GENERATOR SHAFT TORQUE
DUE TO FAULTY SYNCHRONIZATION**

A THESIS

**SUBMITTED TO THE DEPARTMENT OF
ELECTRICAL AND ELECTRONIC ENGINEERING, BUET,
IN PARTIAL FULFILMENT OF THE REQUIREMENTS FOR THE DEGREE OF
MASTER OF SCIENCE IN ENGINEERING**

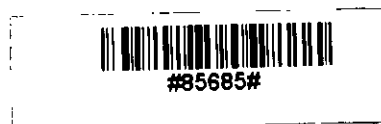
BY

IQBAL KARIM



**DEPARTMENT OF ELECTRICAL AND ELECTRONIC ENGINEERING
BANGLADESH UNIVERSITY OF ENGINEERING AND TECHNOLOGY**

NOVEMBER, 1992



629.165
1992
198

DEDICATED TO MY PARENTS


Declaration

No portion of this work has been submitted to any other University or similar institution for award of any degree.

Countersigned by :

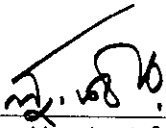
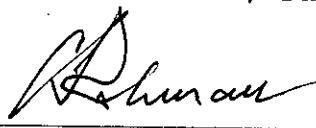
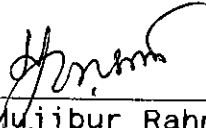

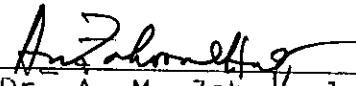

(Dr. S. M. Lutful Kabir)

Supervisor


(Iqbal Karim)

Accepted as satisfactory in the partial fulfilment of the requirements for the degree of Master of Science in Engineering (Electrical and Electronic).

BOARD OF EXAMINERS

1. 
(Dr. S. M. Lutful Kabir)
Associate Professor
Department of Electrical and
Electronic Engineering
BUET, Dhaka-1000, Bangladesh.
Chairman
(Supervisor)
2. 
(Dr. Syed Fazl-i Rahman)
Professor and Head
Department of Electrical and
Electronic Engineering
BUET, Dhaka-1000, Bangladesh.
Member
(Ex-officio)
3. 
(Dr. M. Mujibur Rahman)
Professor
Department of Electrical and
Electronic Engineering
BUET, Dhaka-1000, Bangladesh.
Member
4. 
(Dr. Mohammad Ali Chowdhury)
Assistant Professor
Department of Electrical and
Electronic Engineering
BUET, Dhaka-1000, Bangladesh.
Member
5. 
(Dr. A. M. Zahoorul Huq)
319, Baitul Aman Housing Society
Road No : 6, Shamoli, Dhaka
Bangladesh.
Member
(External)

CONTENTS

Acknowledgements	1
Abstract	ii
List of Figures	iii
List of Symbols	v
CHAPTER 1. INTRODUCTION	
1.1 The Problem	1
1.2 Simulation of faulty synchronization	3
1.3 Representation of saturation within a machine	7
1.4 Scope of the present work	9
CHAPTER 2. MATHEMATICAL FORMULATION	
2.1 State space model	11
2.2 Modelling synchronous machine	11
2.3 Modelling the shaft assembly	15
2.4 Modelling automatic voltage regulator	17
CHAPTER 3. SHAFT TORQUE DUE TO FAULTY SYNCHRONIZATION	
3.1 Introduction	20
3.2 Approximate analysis of shaft torques	21
3.3 Computer program for the simulation of faulty synchronisation	24
3.4 Instantaneous responses following faulty synchronisation	25
3.5 Simulation of shaft torque for different synchronising angles	26

3.6	Effect of machine parameters on shaft torque	28
3.7	Effect of network parameters on shaft torque	29
CHAPTER 4. EFFECT OF SATURATION ON SHAFT TORQUE		
4.1	Incorporation of saturation in the model	30
4.2	Mathematical background	30
4.3	Leakage path saturation model	32
4.4	Mutual path saturation model	33
4.5	Effect of saturation of machine parameters on shaft torque	34
CHAPTER 5. COMPARISON BETWEEN FAULTY SYNCHRONIZATION AND SHORT CIRCUIT		
5.1	Introduction	37
5.2	Simulation of fault throwing test	38
5.3	Effect of fault duration on peak-to-peak torque	39
5.4	Effect of fault location on peak-to-peak torque	40
5.5	Comparison of faulty synchronisation and short circuit	41
CHAPTER 6. CONCLUSION AND FURTHER WORK		
6.1	Conclusion	44
6.2	Further work	45
REFERENCES		47
APPENDICES		51
TABLES		57
FIGURES		60

Acknowledgement

The author wishes to express his sincere thanks and gratitude to his supervisor Dr. S. M. Lutful Kabir for his guidance, co-operation, spontaneous encouragement and many helpful discussions throughout this work and without whose efforts the work would not have been completed.

The author is grateful to Dr. Mohammad Ali Chowdhury for his inspiration and assistance. He is also indebted to the Head of the Department and other teachers and employees for helping in many ways to complete the work, specially for providing the facilities of microcomputers in the department.

The author also thanks his colleagues of Bangladesh Power Development Board for their help and support during the work. Finally he also thanks the University authority for bearing the expense of this work.

Abstract

The generator shaft designers usually consider the shaft torques that develop during short circuit as the most severe case. But, recent studies show that the developed torques due to faulty synchronisation could be greater than that occur during short circuit. This thesis describes a method of simulating faulty synchronisation of a generator with a power system. Previous studies, in almost all cases, neglected the effects of generator saturation in the process of simulation. Even included, the saturation only in the mutual paths of a generator was considered. But since the currents involved during faulty synchronisation become quite large for some synchronising angle, the leakage paths may also saturate. The simulation of faulty synchronisation described in this thesis includes saturation both in the mutual and leakage path of a generator. It has been demonstrated that a considerable change in results occur if saturations in a generator are neglected.

A comparison between the phenomena of faulty synchronisation and that of short circuit has also been incorporated in the work. For this purpose, the shaft torques developed during fault throwing test under varying conditions are studied. The results reveal that the shaft designers should consider the magnitude of torques developed during faulty synchronisation as one of the design criterion of turbine generator shaft system.

List of Figures

- 2.1 The equivalent circuit of synchronous machine
- 2.2 Electrical network for the system studied
- 2.3 Representation of the shaft assembly
- 1.4 Block diagram of an Automatic Voltage Regulator
- 3.1 Approximate representation of the electrical system
- 3.2 T-section equivalent circuit of the turbine-generator shaft system
- 3.3 Flow diagram of the computer program for study on faulty synchronization
- 3.4 Time response of machine 'A' during out-of-phase synchronization of 120 degree, machine voltage leading transformer voltage
- 3.5 Time response of machine 'A' during out-of-phase synchronization of 120 degree, machine voltage lagging transformer voltage
- 3.6 Maximum current following out-of-phase synchronization for machine 'A'
- 3.7 Peak-to-peak shaft torque following out-of-phase synchronization for machine 'A'
- 3.8 Effect of machine parameter on peak-to-peak quill-shaft torque following out-of-phase synchronization
- 3.9 Effect of network parameter on peak-to-peak quill-shaft torque following out-of-phase synchronization

- 4.1 Simulation of fault throwing test on machine 'A'
- 4.2 Effect of fault duration on peak-to-peak values during fault throwing test
- 4.3 Effect of fault location on peak-to-peak torques during short circuit period
- 4.4 Effect of fault duration on peak-to-peak torques after fault clearance
- 5.1 Leakage path saturation characteristics
- 5.2 Shackshaft's method of calculating mutual reactances
- 5.3 Effect of saturation on maximum stator current following out-of-phase synchronization of machine 'A'
- 5.4 Effect of saturation on peak-to-peak air-gap torque following out-of-phase synchronization of machine 'A'
- 5.5 Effect of saturation on peak-to-peak quill-shaft torque following out-of-phase synchronization of machine 'A'
- 5.6 Effect of saturation on peak-to-peak coupling-shaft torque following out-of-phase synchronization of machine 'A'

List of Symbols

- X_d = Direct-axis synchronous reactance
- X'_d = Direct-axis transient reactance
- X''_d = Direct-axis subtransient reactance
- X_q = Quadrature-axis synchronous reactance
- X''_q = Quadrature-axis subtransient reactance
- T'_d = Direct-axis transient short circuit time constant
- T''_d = Direct-axis subtransient short circuit time constant
- T''_q = Quadrature-axis subtransient short circuit time constant
- R_a = Armature resistance
- X_a = Armature reactance
- X_{md} = Direct-axis magnetizing reactance
- X_{kf} = Mutual reactance between field and damper
- X_{kd} = Direct-axis damper reactance
- R_{kd} = Direct-axis damper resistance
- X_f = Field reactance
- R_f = Field resistance
- V_f = Field voltage
- X_{mq} = Quadrature-axis magnetizing reactance
- X_{kq} = Quadrature-axis damper reactance
- R_{kq} = Quadrature-axis damper resistance

V_d = Direct-axis component of synchronous machine voltage
 V_q = Quadrature-axis component of synchronous machine voltage
 V_{bd} = Direct-axis component of bus-bar voltage
 V_{bq} = Quadrature-axis component of bus-bar voltage
 i_d = Direct-axis component of armature current
 i_q = Quadrature-axis component of armature current
 i_f = Field current
 I_a = Armature current
 ψ = Flux terms
 ω_0 = Synchronous speed
 ω = Rotor speed
 ω_m = Mechanical system oscillation frequency
 δ = Rotor angle
 p = Derivative with respect to time
 T_e = Electromagnetic air-gap torque
 T_q = Quill-shaft torque
 T_c = Coupling-shaft torque
 T_m = Mechanical torque due to turbine input
 J_1 = Moment of inertia of the generator
 J_2 = Moment of inertia of the reduction-gear
 J_3 = Moment of inertia of the turbine
 K_1 = Inverse of torsional spring constant of the quill-shaft
 K_2 = Inverse of torsional spring constant of the coupling-shaft

X_{un} = Unsaturated leakage reactance

X_{st} = Saturated leakage reactance

I_{un} = Current at which leakage reactance starts to saturate

I_{st} = Current at which leakage reactance becomes saturate

X_i = Reactance at an intermidiate point between 'd' and 'q' axis

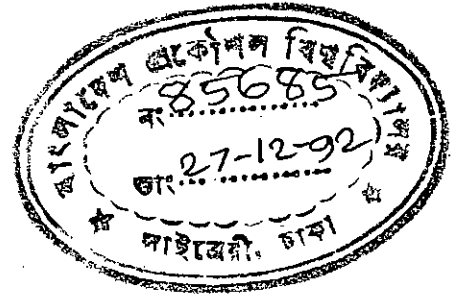
$X_{m ds}$ = Saturated d-axis mutual reactance when flux is on d-axis

$X_{m qs}$ = Saturated q-axis mutual reactance when flux is on q-axis

X_{sd} = Difference between $X_{m ds}$ and $X_{m qs}$

$X_{m d}$ = Saturated d-axis mutual reactance

$X_{m q}$ = Saturated q-axis mutual reactance



CHAPTER 1

INTRODUCTION

1.1 The Problem.

A power system often experiences planned or unplanned disturbances, the nature of which are either transient or harmonic. Transient disturbances may result from short circuit faults, transmission line switching or out-of-phase synchronization. Harmonic disturbances may be caused by an instability of power flow in the grid or by sub-synchronous resonance arising from series capacitor compensated tie-line. Whether transient or harmonic, variation in electrical current and power occur following a disturbance. The variation is, consequently, transformed into variation in electromagnetic torque within the generators of the system due to interaction between air-gap fluxes and currents in the generator. The electromagnetic torque produces torsional stresses on rotors of the turbine-generator shaft system. An exact knowledge of the torsional stresses following different disturbances is, therefore, of great importance in designing generator and turbine shafts.

For many years, short circuit fault has been considered to be the most severe disturbance and the torsional stresses developed during the fault has been the criteria of shaft design. American National Standard Institute (ANSI) [1] specifies that mechanical strength of shaft system should be such that the generator is capable of withstanding without mechanical injury during any type of short circuit at its terminals, for a duration within which short circuit thermal requirement does not exceed. While the generator shafts are being designed on the basis of short circuit torsional limit, there has been increasing recognition of faulty synchronization being a source of producing more severe shaft torque than short

circuit. The realization came through several incidents of shaft failure during faulty synchronization at different places.

In August 1974, two 1300 MW generators of American Electric Power Service Corporation [2] suffered shaft damage when one of the two generators was attempted to bring into synchronism with the system. The shafts of both the generators were twisted and a third 800 MW machine connected to the system experienced significant shock. In May 1976, the shaft of a 955 MVA generator [3] had severely been damaged due to faulty synchronization. It occurred when the generator was inadvertently switched on to a stiff 345 kV grid in out-of-phase. From relaying response, it was known that breaker closing occurred with the generator voltage leading system voltage by about 120 electrical degree. In the same year, the load coupling shafts of two 21 MW gas turbine units in an installation of Consumers Power Company were damaged [4]. In one unit, the load coupling shaft was twisted until it fractured. In the other unit, the shaft was damaged due to twisting but fracturing did not occur. Although there was evidence that the shaft failures occurred during synchronization, there was no evidence of damaging of the stator windings due to excessive current. In the incident of Consumer Power Company, the failure of the load coupling shaft due to large instantaneous torques without evidence of expected excessive currents in the stator windings was then considered highly unlikely.

At home, in April 1990, two 33 MW generators of Haripur power station of Bangladesh Power Development Board were damaged during synchronization. The two units at Haripur were connected with the grid through a step-up transformer.

Due to a disturbance in the grid the high-tension side breaker of the transformer tripped. The generators thus became isolated from the system. After a short while, it was attempted to synchronize the units by reclosing the high-tension side breaker of the transformer. But unfortunately, the synchronization was not proper. Consequently the quill shafts of both the units were found to be twisted.

The incidents described above demonstrate how severe torque could be developed in the mechanical system during faulty synchronization. In order to protect the system from serious consequences following disturbances, different protecting equipments are developed. These development have been enabled through an intimate understanding of system behavior, particularly in the presence of the disturbances. The obvious way of obtaining knowledge is from tests on the system itself. But these would induce the failure which is wished to prevent and so models have to be used. Digital computer models could be employed in order to simulate the phenomena following faulty synchronization. The simulation through the models should provide an overview of the phenomena and depending on the severity and possible consequences of the event, measures could be undertaken to avoid the shaft failure. Moreover, accurate prediction of torsional vibration due to faulty synchronization should establish a guideline for engineers, engaged in shaft design.

1.2 Simulation of faulty synchronization.

The analysis on the phenomena arising from out-of-phase synchronization has been the subject of much work. The first attempt to simulate the situation involved analogue computers [5]. This proved quite successful particularly with the

introduction of operational amplifier technology [6]. But the use of analogue computers declined with the advent of the digital computer which offered flexibility in operation. The digital computer provided the facilities to undertake studies with various form of machine and shaft system representation.

A. J. Wood [7], in his study on out of phase synchronization, represented the generator by an equivalent circuit often referred to as 'constant emf behind transient reactance' representation. The representation is based on Doherty's first principle [8]. Expressions for current and electromagnetic torque as a function of synchronizing angle and system reactance were developed. The calculated maximum electromagnetic torque was then used to determine maximum mechanical shaft torque. The values for various switching angles and system reactances were also calculated. It was shown that the maximum electrical torque occurred for a switching angle of around 120 electrical degree. Since the assumption of constant emf is only valid during first few cycle after the initiation of fault, the outcome of his study did not provide accurate results. The shaft of the system under study was modeled by a single lumped mass. The model was too simple to give accurate representation of the actual mechanical system.

The two axis d-q model of R. H. Park [9] overcame the inadequacy of the simple model. In the d-q model, the synchronous machine is resolved into two coil equivalent turning in synchronism with its rotor. One coil remains aligned with the field or the direct axis and the other is displaced by 90 degrees to the field or the quadrature axis. The two axis equivalent machine is then represented by two electrical networks. Reactances associated with the various windings are

represented by their leakage and mutual components and resistances are represented in series with the leakage reactances. P. C. Krause et al [10], J. V. Mitche et al [11], T. J. Hammons [12-14] and others have used d-q model to represent generators in their study on faulty synchronization.

P. C. Krause et al [10] considered a system of two machine infinite bus bar system. The two synchronous machines were simulated using Park's equations with two damper windings in the quadrature axis. Conventional equivalent circuits were used in representing the two axis of the machine. Each machine was coupled with IEEE type 1 excitation system [15]. The turbine generator shaft systems were represented by rotating inertia and torsional compliance. The study of P. C. Krause et al revealed that the out-of-phase synchronization could produce severe instantaneous shaft torque.

J. V. Mitche et al [11] simulated an incident of faulty synchronization of a 4-pole 955 MVA turbine generator. The synchronous machine was modeled using Park's equations at the sub-transient level [16]. The turbine section and connecting shafts were simulated by a five element lumped-mass-spring model with a 1 percent mutual damping between masses. The instantaneous air-gap and shaft torque following synchronization were simulated for the incident. Discrepancies between the simulated and the recorded results were observed. The discrepancies are thought to be due to using approximate machine model and neglecting saturation within the machine.

Several studies on faulty synchronization had been made by T. J. Hammons [12-14]. In one of his studies, T. J. Hammons [12] produced detailed torque char-

acteristics for two typical 660 MW and a 300 MW turbine generators during faulty synchronization. The generators in the Hammons work were simulated by two axis conventional equivalent circuits, the parameters of which were obtained from three-phase short circuit tests. Mass-spring model was used in simulating turbine-generator shaft system. In his study, an elaborate investigation on the effects of three phase faults and faulty synchronization on the mechanical stressing of large turbo-generators was made by T. J. Hammons [13]. Like others, the investigation shows that synchronization at an angle of approximately 120 degree gives rise to high shaft torque. In another study [14], T. J. Hammons stressed on the importance of modeling damper in the simulation of faulty synchronization, since it has significant influence on torsional vibrations of turbine-generator shafts.

Although the machine representation by d-q model was quite acceptable, the value of the machine parameters to be used for the model became a matter of serious controversy. This was because of uncertainty of extracting parameters from test results. Conventionally, the current response following a three-phase short circuit at the machine terminal is analyzed in determining equivalent circuit parameters. The conventional method of parameter measurement was first reviewed by Adkins [17] and then by Shackshaft [18]. But Canay [19] differed with Adkins and Shackshaft in representing the mutual reactance between field and damper. The parameters obtained following Canay's approach gave the best results in simulating different tests [20]. But studies on faulty synchronization made so far, did not include the Canay's model in representing the machine.

1.3 Representation of saturation within a machine.

Most of the studies described so far used constant values of machine parameters. But in reality due to changes in the level of saturation of iron within the machine, these values change as a machine's voltages and currents exceed certain levels. The variations suffered by these parameters have to be included in the simulation of faulty synchronization if accurate results are to be achieved. To do this, requires a detailed knowledge as to how the various machine inductances change with saturation.

The accurate prediction of iron saturation in synchronous machine and, therefore, of machine reactance have been dealt by many investigators. The use of saturation factor to correct mutual reactances has been widely accepted [21]. Direct-axis magnetization characteristics are, often, employed to determine a common saturation factor for both 'd' and 'q' axes. But experiment [22] shows that the q-axis saturates more than the d-axis. Shackshaft [23] recognized this in his model of mutual path saturation for large alternators. In his model, for a given air-gap voltage he calculates the mutual reactances of the machine from magnetization characteristics of 'd' and 'q' axes. The reactances are then modified from the knowledge of position of the rotor flux. Hence the resultant d- and q-axis mutual reactances are each functions of the magnitudes and position of the rotor flux.

Whilst a reasonable amount is known about saturation of the main flux path, little is known about saturation of the leakage paths. This is so, because there is no satisfactory test capable of isolating leakage path effects. The effect of

leakage path saturation is apparent by the fact that transient reactances reduce in magnitude as short circuit currents increase in magnitude [24,25]. Kilgore [24] and Concordia [25] postulated that the reduction in transient reactances occurred in two parts. The first is due to saturation in the main magnetic path and the second to saturation in leakage paths.

A broad assessment of the sensitivity of a machine's parameters to saturation can be made with the aid of finite element methods [26-28]. By virtue of its very nature, the method is highly time consuming. But as computing power increases the technique has become useful as a means of parameter assessment. Macdonald et al [26] applied the method to evaluate steady-state reactances and investigated the variations of both d- and q-axis values with load and power factor. Flores et al [27] investigated the effect of saturation on armature leakage reactance which was found to fall by 12-25 percent of its unsaturated value as stator current increases to 5 pu. Turner et al [28] have simulated flux decay and three-phase short circuit tests using the method. Difficulties in using the finite-element method directly for operational and in particular transient analysis, lie with the amount of computer time and capacity needed to cover a reasonable time span of investigation.

No significant work has been carried out to investigate the effect of saturation on developing shaft stresses during faulty synchronization. Although some studies considered the saturation on the main flux path only, no comparison has ever been made on the differences in responses with and without considering the effects. More importantly, recent studies [18] revealed that the effect of leakage

path saturation has a great influence on dynamic performance of machine. Hence an elaborate study should be made on the effect of saturation both in the main and leakage path during disturbances due to faulty synchronization.

1.4 Scope of the present work.

The analysis on faulty synchronization carried out so far, are all different in one way or another. None of the analysis can be considered as a complete one. In order to obtain a comprehensive understanding of the event, one should consider all aspects of electrical and mechanical system representation in the modeling process. The form of equivalent circuit and its associated parameters should be properly selected in order to represent the machine accurately. Once the basic representation of the machine is ensured, the variation of the parameters with the change in saturation level should also be accurately accounted for. The overall accuracy of the simulation depends not only on the machine representation but also on the representation of the mechanical components contributing to the development of shaft stresses during faulty synchronization.

Considering the above mentioned requirements, the author has been asked to incorporate equivalent circuits of the machine having accurate form, the validity of which has sufficiently been established. The parameters to be used for the equivalent circuit should be available from works test results. In addition to using proper equivalent circuit, the simulation should incorporate the effect of both mutual and leakage path saturation in the transient state following faulty synchronization. A comparison has to be made between the simulations with and without incorporating the saturation effects.

The author's second task was to carry out a study on shaft torque developed during short circuits as well as during removal of short circuits. This study would facilitate to assess the relative importance of two phenomenon namely short circuit and faulty synchronization.

CHAPTER 2

MATHEMATICAL FORMULATION

2.1 State space model.

State space modeling is a method of solving differential equations in a step by step manner. If a system is characterized by a set of differential equations having minimum number of state variable, the system can be described in a state space form. When the set of equations contain an n th order differential equation, it is transformed into 'n' number of simultaneous first order differential equations. In state space form the rate of change of a particular variable is expressed as a function of other variables including itself. Similar equations are arranged for other state variables. In order to calculate the responses of the variables for a given condition, the state equations are used in conjunction with the equations for the control variables, if any. In a particular time step the rate of changes are determined from the knowledge of the values of the variables obtained in the previous step. This rate of change gives the new value of the variables. The procedure is repeated for the consecutive time steps. An elaborate form of state space model for the problem at hand is described in the following sections.

2.2 Modelling synchronous machine.

The fundamental electromagnetic interaction within a synchronous machine is described mathematically by a set of differential equations. The equations are based on two axis equivalent representation of a machine. The equivalent circuits as suggested by Canay [19] in the two axes are given in Figure 2.1. Figure 2.1a is the equivalent circuit for direct axis and Figure 2.1b for the quadrature axis. Referring to Figure 2.1, V_f corresponds to excitation voltage of the machine. Reactances associated with the various windings are represented by X_o ,

X_f , X_{kd} , X_{kq} corresponding to armature, field and damper leakages respectively. X_{md} , X_{mq} represent mutual coupling between stator and rotor circuit and X_{kf} represents coupling between field and damper. The letter R represents various resistances.

The direct and quadrature axis voltages of the synchronous machine, V_d and V_q are given by [29] :

$$V_d = p\psi_d + \omega\psi_q + R_a i_d \quad (2.1)$$

$$V_q = p\psi_q - \omega\psi_d + R_a i_q \quad (2.2)$$

where ' ω ' is the rotor speed and is related to synchronous speed ' ω_0 ' as $\omega = \omega_0 - p\delta$. The ' $\omega\psi$ ' terms represent voltage induced in one axis by virtue of flux in the other axis due to 'rotational voltage' whilst ' $p\psi$ ' terms represent voltage induced in one axis due to rate of change of flux in the same axis, often referred to as 'transformer voltage'.

For the analysis of faulty synchronization the machine is considered to be connected with the infinite busbar through a transformer and a transmission line as shown in Figure 2.2. The terminal voltages of the machine can be related to the infinite busbar voltage as follows :

$$V_d = V_{bd} - \frac{X}{\omega_0} p i_d - R i_d - X i_q + \frac{X}{\omega_0} p \delta i_q \quad (2.3)$$

$$V_q = V_{bq} - \frac{X}{\omega_0} p i_q - R i_q + X i_d - \frac{X}{\omega_0} p \delta i_d \quad (2.4)$$

where R and X are the resistive and reactive parts of the total impedance between the infinite bus and the terminal of the machine. Combining equation (2.3) with

(2.1) and (2.4) with (2.2), the voltage components of the infinite busbar are expressed as :

$$V_{bd} = p\psi_d + \omega_0\psi_q - \psi_q p\delta + R_a i_d + \frac{X}{\omega_0} p i_d + R i_d + X i_q - \frac{X}{\omega_0} p\delta i_q \quad (2.5)$$

$$V_{bq} = p\psi_q - \omega_0\psi_d + \psi_d p\delta + R_a i_q + \frac{X}{\omega_0} p i_q + R i_q - X i_d + \frac{X}{\omega_0} p\delta i_d \quad (2.6)$$

The voltages on the rotor circuits of the machine are expressed as :

$$\text{field} : V_f = p\psi_f + R_f i_f \quad (2.7)$$

$$d - \text{damper} : V_{kd} = p\psi_{kd} + R_{kd} i_{kd} \quad (2.8)$$

$$q - \text{damper} : V_{kq} = p\psi_{kq} + R_{kq} i_{kq} \quad (2.9)$$

The currents are related to the fluxes [29] for 'd' and 'q' axes by two sets of equations in the form of $[\omega_0\psi] = [Z].[I]$, where $[\omega_0\psi]$, $[Z]$, and $[I]$ are the flux, impedance, and current matrices respectively. The set of equations for the d-axis is :

$$\begin{bmatrix} \omega_0\psi_d \\ \omega_0\psi_f \\ \omega_0\psi_{kd} \end{bmatrix} = \begin{bmatrix} X_{md} + X_a & X_{md} & X_{md} \\ X_{md} & X_{md} + X_f + X_{kf} & X_{md} + X_{kf} \\ X_{md} & X_{md} + X_{kf} & X_{md} + X_{kd} + X_{kf} \end{bmatrix} \begin{bmatrix} i_d \\ i_f \\ i_{kd} \end{bmatrix} \quad (2.10)$$

And the set of equations for the q-axis is :

$$\begin{bmatrix} \omega_0\psi_q \\ \omega_0\psi_{kq} \end{bmatrix} = \begin{bmatrix} X_{mq} + X_a & X_{mq} \\ X_{mq} & X_{mq} + X_{kq} \end{bmatrix} \begin{bmatrix} i_q \\ i_{kq} \end{bmatrix} \quad (2.11)$$

Inversion of the impedance matrices of the above relationship gives the currents in terms of fluxes. So the currents in the d-axis are :

$$\begin{bmatrix} i_d \\ i_f \\ i_{kd} \end{bmatrix} = \begin{bmatrix} Y_d(1,1) & Y_d(1,2) & Y_d(1,3) \\ Y_d(2,1) & Y_d(2,2) & Y_d(2,3) \\ Y_d(3,1) & Y_d(3,2) & Y_d(3,3) \end{bmatrix} \begin{bmatrix} \omega_0 \psi_d \\ \omega_0 \psi_f \\ \omega_0 \psi_{kd} \end{bmatrix} \quad (2.12)$$

And the currents in the q-axis are :

$$\begin{bmatrix} i_q \\ i_{kq} \end{bmatrix} = \begin{bmatrix} Y_q(1,1) & Y_q(1,2) \\ Y_q(2,1) & Y_q(2,2) \end{bmatrix} \begin{bmatrix} \omega_0 \psi_q \\ \omega_0 \psi_{kq} \end{bmatrix} \quad (2.13)$$

The equations (2.12) and (2.13) can be written in short :

$$[I]_d = [Y]_d [\omega_0 \psi]_d \quad (2.14)$$

$$[I]_q = [Y]_q [\omega_0 \psi]_q \quad (2.15)$$

The currents in equation (2.5) to (2.9) when replaced by set of equations (2.14) and (2.15), the only type of variables remains in the equations are flux variables. From the resultant equations the 'pψ' terms for different winding can be expressed as a function of fluxes. The final form of the equations is given by [29] :

$$[\dot{X}] = [A][X] + [F] + [B][Z] \quad (2.16)$$

where [X] is the matrix representing state variables which are flux in this case and [Z] is the control matrix, the element of which is the field voltage. The elements of the different matrices of the equation (2.16) are given in Appendix-A.

The developed airgap torque within the machine is expressed as :

$$T_e = \frac{\omega_0 (\psi_d i_q - \psi_q i_d)}{2} \quad (2.17)$$

which becomes the input quantity for the mechanical system. The equations relating the mechanical system and the resultant state space model for the system are described in the next section.

2.3 Modelling the shaft assembly.

A schematic diagram of the shaft assembly for a gas-turbine generator is shown in Figure 2.3a. It consists of three lumped inertias namely generator, reduction-gear and gas-turbine. The generator is connected with the reduction gear by a shaft having negligible per unit mass, which is called quill shaft. And a similar shaft namely load coupling shaft connects the turbine with the reduction gear.

In order to form a state space model for the the system described, an analogous electrical network is formed for the shaft assembly. The network is shown in Figure 2.3b. The inductances are analogous to the moment of inertia of the three lumped masses J_1 , J_2 and J_3 . K_1 and K_2 are the inverse of torsional spring constants or stiffness for the interconnecting shafts. T_e represents the electromagnetic airgap torque which acts as the input to the mechanical system and T_m corresponds the resisting mechanical torque arises due to turbine input. T_q and T_c are the torques developed in the quill shaft and that in the load coupling shaft respectively. The angular velocities corresponding the three lumped mass are described by ω_1 , ω_2 and ω_3 .

The equations for the three loops of the analogous network represent the mechanical equation of machine. They are :

$$T_e = J_1 \frac{d\omega_1}{dt} + K_1 \int (\omega_1 - \omega_2) dt \quad (2.18)$$

$$0 = J_2 \frac{d\omega_2}{dt} + K_1 \int (\omega_2 - \omega_1) dt + K_2 \int (\omega_2 - \omega_3) dt \quad (2.19)$$

$$0 = J_3 \frac{d\omega_3}{dt} + K_2 \int (\omega_3 - \omega_2) dt + T_m \quad (2.20)$$

Substituting ' ω ' with $\frac{d\delta}{dt}$ where ' δ ' is the rotor angle, the above equations (2.18) to (2.20) becomes :

$$T_e = J_1 \frac{d^2\delta_1}{dt^2} + K_1(\delta_1 - \delta_2) \quad (2.21)$$

$$0 = J_2 \frac{d^2\delta_2}{dt^2} + K_1(\delta_2 - \delta_1) + K_2(\delta_2 - \delta_3) \quad (2.22)$$

$$0 = J_3 \frac{d^2\delta_3}{dt^2} + K_2(\delta_3 - \delta_2) + T_m \quad (2.23)$$

When the second order differential terms for the rotor angles are separated out, the resulting equations are :

$$\frac{d^2\delta_1}{dt^2} = -\frac{K_1}{J_1}\delta_1 + \frac{K_1}{J_1}\delta_2 + \frac{T_e}{J_1} \quad (2.24)$$

$$\frac{d^2\delta_2}{dt^2} = +\frac{K_1}{J_2}\delta_1 - \frac{K_1 + K_2}{J_2}\delta_2 + \frac{K_2}{J_2}\delta_3 \quad (2.25)$$

$$\frac{d^2\delta_3}{dt^2} = +\frac{K_2}{J_3}\delta_3 - \frac{K_2 + K_3}{J_3}\delta_2 - \frac{T_m}{J_3} \quad (2.26)$$

Since the above equations are of second order, the solution in state space form is performed by using two first order equations for each second order equation. The detailed representation of the state space model for the mechanical system is given in Appendix-B.

2.4 Modelling automatic voltage regulator.

The purpose of automatic voltage regulator (AVR) is to hold the terminal voltage of the alternator at a prescribed value. There are many types of AVR in use but they all have the same basic principle. The principle is to compare machine terminal voltage with a reference value to obtain an error signal, which after amplification, regulates the machine's excitation. The author, in his work considered an exciter system similar in form to that designated 'type 1' by the IEEE committee concerned with the modelling of excitation system [15].

A block diagram of an AVR is shown in Figure 2.4. Here the terminal voltage of the alternator, V_T is compared with the reference signal, V_{ref} at the error detector-1, where a negative feedback signal ' e_1 ' is added giving a signal at the input of the amplifier block, thus :

$$e_i = V_{ref} - V_T - e_1 \quad (2.27)$$

The amplifier has a gain of K_A and a time constant of T_A so its output is given by :

$$e_2 = \frac{K_A}{1 + sT_A} e_i \quad (2.28)$$

Combining equations (2.27) and (2.28), the derivative of ' e_2 ' is found to be :

$$\dot{e}_2 = -\frac{K_A}{T_A} e_1 - \frac{1}{T_A} e_2 + \frac{K_A(V_{ref} - V_T)}{T_A} \quad (2.29)$$

The amplifier's output signal ' e_2 ' is limited by maximum and minimum values, V_{Rmax} and V_{Rmin} , thus :

$$V_{Rmax} < e_2 < V_{Rmin} \quad (2.30)$$

The output from the regulator is applied to main exciter having transfer function, $1/(1 + sT_E)$ together with a saturation function, S_E which is a non-linear feedback element. Thus the input to the exciter is expressed as :

$$e_{ex} = e_2 - S_E e_3 \quad (2.31)$$

The output of the exciter is given by :

$$e_3 = \frac{1}{1 + sT_E} e_{ex} \quad (2.32)$$

The rate of change of 'e₃' can be derived as :

$$\dot{e}_3 = \frac{1}{T_E} e_2 - \frac{(1 + S_E)}{T_E} e_3 \quad (2.33)$$

In order to maintain stability of the AVR systems a damping function $sK_F/(1 + sT_F)$ is introduced. Thus the output of the feedback block 'e₁' is expressed as

$$e_1 = \frac{sK_F}{1 + sT_F} e_3 \quad (2.34)$$

Simplifying equation (2.34) in conjunction with (2.33), the expression for the derivative of 'e₁' is obtained as :

$$\dot{e}_1 = -\frac{1}{T_F} e_1 + \frac{K_F}{T_F T_E} e_2 - \frac{K_F(1 + S_E)}{T_F T_E} e_3 \quad (2.35)$$

The differential equations (2.35), (2.29) and (2.33) can be arranged in state space model as :

$$\begin{bmatrix} \dot{e}_1 \\ \dot{e}_2 \\ \dot{e}_3 \end{bmatrix} = \begin{bmatrix} \frac{-1}{T_F} & \frac{K_F}{T_F T_E} & \frac{-K_F(1+S_E)}{T_F T_E} \\ \frac{-K_A}{T_F} & \frac{-1}{T_A} & 0 \\ 0 & \frac{-1}{T_E} & \frac{-(1+S_E)}{T_E} \end{bmatrix} \begin{bmatrix} e_1 \\ e_2 \\ e_3 \end{bmatrix} + \begin{bmatrix} 0 \\ \frac{K_A(V_{ref} - V_T)}{T_A} \\ 0 \end{bmatrix} \quad (2.36)$$

At each step the new value of field voltage V_f obtained from e_3 multiplied by a scaling factor S_c is fed into the machine model as terminal voltage V_T is changed.

CHAPTER 3

SHAFT TORQUE DUE TO FAULTY SYNCHRONIZATION

3.1 Introduction.

The effect of faulty synchronization on shaft torque has been investigated by simulating synchronization of one machine having improper phase relationship with an infinite bus-bar of a power system. The one line diagram of the system considered for the study is shown in Figure 2.2. The generator is connected to the system bus-bar through the generator-transformer and a section of line. The short-circuit machine parameters were obtained from reference [10]. The equivalent circuit parameters were then calculated from the short-circuit parameter using Canay's equivalent circuit [19]. The values are shown in Figure 2.1. The equivalent circuit for the mechanical system is shown in Figure 2.3. The data for the elements of the circuit were collected from the same reference [10]. The values are shown in Figure 2.3b.

In the simulation of synchronization, the steady-state condition before synchronization was maintained by setting both machine's open-circuit voltage and infinite bus-bar voltage at 1.0 pu. The machine was synchronized at the low tension side of the generator-transformer. The synchronization angle was simulated by providing a phase difference between the machine's terminal voltage and the infinite bus-bar voltage. At time $t = 0^+$, all the phases of the circuit breaker at the low tension side of the transformer were assumed to be closed simultaneously. The responses of electrical and mechanical quantities following the synchronization were calculated and studied.

3.2 Approximate Analysis of Shaft Torques.

The approximate expression of shaft torque can be derived by analyzing the response of the mechanical system due to an input of electromagnetic air-gap torque. The approximate representation of the electrical system is shown in Figure 3.1, where X'_d and R_a are the transient reactance and armature resistance of the machine and X_l and R_l are the total reactance and resistance between machine terminal and infinite bus-bar respectively. Neglecting the resistances the current phasor is given by :

$$\begin{aligned} I &= \frac{|V| \angle \delta - |V| \angle 0}{|X| \angle 90} \\ &= \frac{|V|}{|X|} \angle \delta - 90 - \frac{|V|}{|X|} \angle -90 \end{aligned} \quad (3.1)$$

where X is the total reactance of the system. Thus the phasor of electrical developed power is :

$$\begin{aligned} P &= VI^* \\ &= \frac{|V|^2}{|X|} \angle 90 - \delta - \frac{|V|^2}{|X|} \angle 90 \end{aligned} \quad (3.2)$$

Since in per unit sense, the expression for power and that of torque are identical, so the expression for instantaneous air-gap torque is given by :

$$T_e = \frac{|V|^2}{|X|} \{ \sin(\omega t + 90 - \delta) - \sin(\omega t + 90) \} \quad (3.3)$$

The above expression can be written as :

$$T_e = \frac{|V|^2}{|X|} m \sin(\omega t + \theta) \quad (3.4)$$

Where $m \cos \theta = \sin \delta$ and $m \sin \theta = \cos \delta - 1$. Taking Laplace on the above equation and after simplification, the Laplace transform of the air-gap torque becomes :

$$T_e(s) = \frac{|V|^2}{|X|} \frac{\omega m \cos \theta + sm \sin \theta}{s^2 + \omega^2} \quad (3.5)$$

From equation (3.4) the peak value of air-gap torque is :

$$\begin{aligned} T_{ep} &= \frac{|V|^2}{|X|} m \\ &= \frac{|V|^2}{|X|} \sqrt{(m \sin \theta)^2 + (m \cos \theta)^2} \\ &= \frac{|V|^2}{|X|} \sqrt{(\cos \delta - 1)^2 + (\sin \delta)^2} \\ &= \frac{2|V|^2}{|X|} \sin \frac{\delta}{2} \end{aligned} \quad (3.6)$$

The exact equivalent circuit for mechanical shaft system is given as in Figure 2.3b. Since the value of moment-of-inertia of reduction gear is small compared with that of generator and turbine, the equivalent circuit can be reduced to a T-section equivalent circuit as shown in Figure 3.2. Where J_e is the moment-of-inertia of the total mass of the turbine-generator system and K_e is the reciprocal of total spring constant. From the T-section equivalent circuit, the equation relating the shaft torque T_s is given by :

$$\frac{1}{J_e} \int_0^t (T_s - T_e) dt + \frac{1}{K_e} \frac{dT_s}{dt} + \frac{1}{J_e} \int_0^t (T_s - 0) dt = 0 \quad (3.7)$$

Taking Laplace on the equation and after simplifications, the Laplace transform of the shaft torque becomes :

$$T_s(s) = \frac{2K_e}{J_e \left(s^2 + \frac{4K_e}{J_e} \right)} T_e(s) \quad (3.8)$$

The complete expression for the shaft torque in s-domain can be obtained by substituting $T_e(s)$ from equation (3.5). Therefore,

$$T_s(s) = \frac{2|V|^2 K_e}{|X| J_e} \frac{\omega m \cos \theta + sm \sin \theta}{(s^2 + \omega^2) \left(s^2 + \frac{4K_e}{J_e} \right)} \quad (3.9)$$

Taking the inverse laplace transform of $T_s(s)$, the time domain solution of $T_s(t)$ can be obtained. The mathematical steps in elaborate form is given in Appendix C and the expression is :

$$T_s(t) = Km \sin(\omega t + \theta) - Km \sin \theta \cos \omega_m t - K \frac{\omega}{\omega_m} m \cos \theta \sin \omega_m t \quad (3.10)$$

where K is a constant and is equal to $\frac{2|V|^2 K_e}{|X| J_e \left(\frac{4K_e}{J_e} - \omega^2 \right)}$ and ω_m is the angular mechanical oscillation frequency and is given by $\sqrt{\frac{4K_e}{J_e}}$. The two mode of oscillation are observed in the expression for $T_s(t)$, one at angular power frequency ω and the other at angular mechanical oscillation frequency ω_m . The peak value of the first term is given by :

$$\begin{aligned} T_{sp1} &= Km \\ &= K \sqrt{(m \sin \theta)^2 + (m \cos \theta)^2} \\ &= K \sqrt{(\cos \delta - 1)^2 + (\sin \delta)^2} \\ &= 2K \sin \frac{\delta}{2} \end{aligned} \quad (3.11)$$

Whereas, the resultant peak of the second and third term is given by :

$$\begin{aligned} T_{sp2} &= K \sqrt{(m \sin \theta)^2 + \left(\frac{\omega}{\omega_m} m \cos \theta \right)^2} \\ &= K \sqrt{(\cos \delta - 1)^2 + \left(\frac{\omega}{\omega_m} \sin \delta \right)^2} \end{aligned} \quad (3.12)$$

The expressions of the peak values are used in explaining the maximum shaft torque that could occur in a machine during faulty synchronization.

3.3 Computer program for the simulation of faulty synchronization.

The mathematical state-space model developed in Chapter 2 has been used to write a FORTRAN program for the simulation of faulty synchronization. A flow diagram followed in development of the program is given in Figure 3.3. The admittance matrix used in step 6 of the diagram was obtained by inverting the impedance matrix formed by machine's equivalent circuit parameters [29]. The solution of the state-space model for the electrical and the mechanical network as used in steps 10 and 11 was made using fourth order Runge-Kutta integration routine.

Four subroutines were used in the development of the program. The first one called XMTRX forms the impedance matrices of the machine. The inputs for the subroutine are the machine's equivalent circuit parameters and its outputs are the d- and q-axis impedance matrices. The second subroutine called AINV performs inversion of a square matrix. Gauss elimination technique was used in developing the routine. The SLOPE subroutine determines the rate of change of a set of first order differential equations. The routine uses a fourth order Runge-Kutta technique in order to determine the slopes. The same subroutine was used for solving both electrical and mechanical state space model. The fourth subroutine called AVR simulates the automatic voltage regulator. The terminal voltage calculated in the main program at each time step is passed as input to the subroutine. The routine then calculates the appropriate field voltage and

supplies the main program.

The program starts with the measured values of initial terminal condition. The values of the terminal quantities namely voltage, current, power, power factor and rotor angle are transformed into steady-state five winding fluxes using phasor relationship between them. The mechanical input power is set equal to zero. As the output of the machine being zero, the pre-disturbance input power is equal to the constant losses within the machine. Since these losses are neglected in the transient state, the mechanical power is assumed to be zero. The terminal voltage being considered as reference, the faulty phase difference is created by imposing a phase angle with the infinite bus-bar voltage. Since the difference in phases between terminal and infinite bus voltage after switching does not match the steady-state condition prior to the disturbance, the fluxes and consequently the currents and air-gap torque changes. The changes are computed by the program developed for a time step of 0.001 second. The particular time step was chosen after observing the results for various time steps of 0.01, 0.001 and 0.0001 seconds. The responses of the derived quantities are stored in the output file for a total time of 0.5 seconds. The outputs are then retrieved from another package program called GRAPHER in order to present the results in graphical form.

3.4 Instantaneous responses following faulty synchronization.

Time responses of the machine following synchronization with a initial phase difference of 120 electrical degree, machine voltage leading transformer voltage, are exhibited in Figure 3.4. The figure includes the instantaneous wave-shapes of stator current, air-gap torque, quill-shaft torque and coupling-shaft torque. The

wave-shape of the stator current and that of electromagnetic air-gap torque are very similar. Their peak values occur during first cycle following synchronization. The interaction between 50 Hz power frequency oscillation and slow natural frequency of mechanical system oscillation is clearly exhibited in the wave-shapes of shaft torque, in which natural frequency of oscillation dominates over the power frequency oscillation. The approximate natural frequency of the mechanical system can be calculated from the equivalent circuit, using the value of the circuit elements. For the study, the value is found to be 8.6 Hz, which also corresponds to the value obtained from the simulated results.

Similar time responses with initial phase difference of 120 degree lagging instead of leading are shown in Figure 3.5. As expected, the only difference in two sets of wave-shapes is the reversal of signs for the quantities shown.

The approximate expression for shaft torque derived in the previous Section 3.2 and given by equation (3.10) shows that the response due to mechanical oscillation is being subtracted from that due to electrical signal. The fact is seen to be reflected in the wave-shapes shown in Figure 3.4. The relative peaks of the two signals are also seen to be in proper proportion as estimated from the derivation.

3.5 Simulation of Shaft torque for different synchronizing angle.

Since the peak-to-peak shaft torque is of great concern for the design engineers, the calculated peak-to-peak torques at different synchronizing angle were studied. The instantaneous values of current and torques similar to those as

shown in Figures 3.4 and 3.5 were computed for synchronizing angles of 30 degree to 330 degree at an interval of 15 degree. The maximum values of stator current and the peak-to-peak values of air-gap torque, quill-shaft torque and coupling-shaft torque were found out from the time responses. The maximum values of current are plotted against synchronizing angle and shown in Figure 3.6. The peak of the maximum currents is found to occur at synchronizing angle of around 180 degree. Similarly the peak-to-peak values of torques are plotted against synchronizing angle as shown in Figure 3.6. The figure shows that the maximum value of peak-to-peak air-gap torque occurred at around 180 degree of synchronizing angle. Whereas, the traces for peak-to-peak shaft torques demonstrate that there are two peaks at different synchronizing angle, one at around 120 degree and other at around 240 degree.

Occurrence of one peak for the air-gap torque and two peaks for the shaft torque can be explained from the derivation given in Section 3.2. Since the air-gap torque is mainly originated due to the electrical disturbance, only the electrical signal determines the peak of the air-gap torque. As given in equation (3.6), the peak value of the electrical torque suggests that the peak would occur at 180 degree. On the other hand, the peaks of the shaft torques are the resultant of two waves, one originating from electrical signal and other from mechanical system oscillation. The expressions for the two components are given in equations (3.11) and (3.12). The resultant peak can be expressed as :

$$T_{,p} = \sqrt{T_{,p1}^2 + T_{,p2}^2} \quad (3.13)$$

The values of δ at which the maximum value of the resultant peaks occurred can

be derived by equating $\frac{dT_{sp}}{d\delta} = 0$. It is found that the maximum value occurs at a δ which satisfy the equation $\cos\delta = -\frac{2\omega_m^2}{\omega^2 - \omega_m^2}$. It is evident from the relationship that there are two maxima, one occurs between 90° and 180° and other between 180° and 270° . The values are in correspondence to the results obtained from the simulation.

3.6 Effect of Machine Parameters on Shaft Torque.

Apart from mechanical parameters for the shaft, the electrical parameters of the machine influence the developed shaft torque during faulty synchronization. In order to investigate the variation of the developed torque due to variation of machine parameter, the investigation explained in Section 3.3 was repeated for a machine having different electrical parameters. The comparative study between two sets of parameters is made in Table 1. The first set of parameters given in column-2 of Table-1 corresponds to parameters of machine 'A' whilst that given in column-3 represent the parameters of machine 'B'.

The peak-to-peak quill-shaft torque developed due to faulty synchronization at different synchronizing angles are plotted in Figure 3.8. Since the response of quill-shaft and coupling-shaft torque are very similar, so only one of them was studied. Figure 3.8 shows that the peak values of the shaft torque for machine 'A' is greater in almost same proportion at different synchronizing angles. The magnitude of the peak shaft torque is determined by the peak air-gap torque. And since the peak air-gap torque is inversely proportional to the reactance between machine's internal voltage and infinite bus-bar voltage [30], the shaft torques are also inversely proportional to the reactance. When the reactance for

the two machines are compared, it becomes apparent that the ratio of peak-to-peak shaft torques as exhibited in Figure 3.8 is approximately same as the inverse ratio of the machine's transient reactances.

3.7 Effect of Network Parameter on Shaft Torque.

The machine when synchronized with a system, the system reactance become a factor in determining the peak shaft torque. In order to investigate the effect of system reactance on the developed torque, the peak-to-peak quill-shaft torque at different synchronizing angle for three different set of network parameter were calculated. The calculated values as a function of synchronizing angle are plotted in Figure 3.9. The figure shows that if the network parameter is increased the peak shaft torque is decreased which is expected because of the explanation given in the previous Section 3.6. Since the network parameter constitute a part of the total reactance in between machine's internal voltage and infinite bus-bar voltage, its effect should be similar to that of machine's transient reactance.

CHAPTER 4

EFFECT OF SATURATION ON SHAFT TORQUE

4.1 Incorporation of saturation in the model.

Each reactance of the equivalent circuits corresponds to a particular magnetic path within the machine. The paths include magnetic material, the permeability of which determines the flow of flux for a given magnetomotive force. The permeability of these paths vary with increasing mmf, due to saturation. The corresponding reactances, therefore, become non-linear. Saturation in the main flux path of the machine is reflected in the machine's magnetization curve. The mutual reactance, which is derived from the curve, reduces gradually as magnetization current increases. Similarly, due to saturation, leakage reactances of windings also reduce as the permeability of the iron surrounding them decreases with the increase in winding current. Flores et al [27] calculated armature leakage reactance, using the finite element method, for different armature currents. The changes in leakage reactances with change in current are fundamentally the same irrespective of winding, because of their common form of flux path surrounding a coil. The problem of accommodating the effect of saturation in the digital model lies in determining how each reactance changes with the machine terminal voltage and current and how to introduce these changes into the calculation of machine performance.

4.2 Mathematical background.

The differential equations describing a machine's fundamental electromagnetic interactions are usually expressed on the assumption that the machine's reactances are constant. Therefore, the use of digital models based on these equations, as described in Section 2.2, is limited to machine operation at relatively low currents

and voltages. The changes in reactances due to saturation effects are sometimes [31,32] incorporated in linear models by varying the values of machine inductances as current and voltage levels change. Introducing discrete changes in reactances implies the occurrence of discrete changes in energy which is not correct because changes in magnetic energy occur continuously, not discretely. Thus the rate of change in reactances must be included in the mathematical equations, along with their associated reactance changes.

The magnetic fluxes in a machine can be expressed in terms of inductances as follows :

$$[\psi] = [L].[i] \quad (4.1)$$

where $[\psi]$, $[L]$ and $[i]$ are flux, inductance and current matrices. The change in flux due to change in both current and inductances can be expressed as :

$$p[\psi] = [L].p[i] + p[L].[i] \quad (4.2)$$

The term $[L].p[i]$ in equation (4.2), which is normally the only term to be incorporated, represents the change in flux due to current change and the other term $p[L].[i]$ represents the change in flux due to inductance change. In the step by step solution of a machine's differential equations as discussed in Section 2.2, the flux changes due to current changes are calculated at each time step and the new flux values thus obtained are used to evaluate the currents. Since,

$$[L].p[i] = p[\psi] - p[L].[i] \quad (4.3)$$

So, flux changes at each step due to current changes can be obtained by subtracting the 'inductance change term' from the 'total change term'. Therefore, the

linear model described in Section 2.2 can be modified into an universal form by simply subtracting the 'inductance change term' from the equations. Since fluxes were chosen as state variable in the present digital model, so the term $p[L].[i]$ has, therefore, to be expressed in terms of instantaneous fluxes. The changed equation is :

$$p[L].[i] = p[L].[Y].[\omega_0\psi] \quad (4.4)$$

Since $[i] = [Y].[\omega_0\psi]$, where $[Y]$ is the admittance matrix of the machine.

4.3 Leakage path saturation model.

In the equivalent circuit of alternator shown in Figure 2.1 leakage is represented by reactances X_a , X_{kf} , X_f , X_{kd} and X_{kt} . A model for leakage path saturation is given in reference [32]. The model describes the variation of leakage reactances according to the magnitude of the corresponding currents. These reactances falls at an increasing rate as current increases. After a certain current, this rate of fall decreases until the final saturated value is reached. The result is that the reactance to current curve has an inverted 'S' shape as shown in Figure 4.1. Referring to Figure 4.1, I_{mn} represents the current at which leakage reactance starts to saturate whilst I_{st} is the value of current at which reactance becomes saturated. The curve can be described mathematically by dividing it into two parts 'AB' and 'BC' with 'B' occupying the mid point between A and C. Portion 'AB' can be represented by an inverse exponential curve whilst portion 'BC' can be represented by a direct exponential curve. The equations for the curves

are developed in reference [32]. The resulting equations are:

$$X_{AB} = a_0 + b_0 \exp\left(-\frac{I_{st} - i}{I_{st} - I_{un}} \cdot f_c\right) \quad (4.5)$$

$$X_{BC} = c_0 + b_0 \exp\left(-\frac{i - I_{un}}{I_{st} - I_{un}} \cdot f_c\right) \quad (4.6)$$

where f_c is termed as the 'curvature factor', since it determines the curvature of inverted 'S' shape. It is apparent that varying I_{un} , I_{st} , X_{st} and f_c , saturation curves of differing 'S' shape can be simulated over particular range of current.

4.4 Mutual path saturation model.

The significant saturation in an alternator is that associated with the main flux path. The non-linear relationship between flux produced in the main path and excitation mmf is apparent from magnetization characteristics. Variations in the value of a machine's main path reactance with excitation are simply derived from its magnetization characteristic. There is no problem in incorporating main flux path saturation in a digital model provided d- and q-axis characteristics are the same. But this is found to be not so, q-axis reactances being less than their d-axis counterparts. Variations in the magnetization reactances of the two axes are thought by some, to be independent of each other, so that reactance changes can be treated according to individual axis mmfs.

Shackshaft investigated that for a given flux, the reactances in the 'd' and 'q' axes will vary as the axis of the resultant flux moves. According to him, the fundamental construction of an alternator determines that the permeance and, therefore, reactance of the main flux path vary sinusoidally between 'd' and 'q'

axes. Thus in Figure 4.2, the value of reactance X_i at an intermediate point between 'd' and 'q' axes is given by:

$$X_i = X_{mds} \cos^2 \theta + X_{mq_s} \sin^2 \theta \quad (4.7)$$

where, X_{mds} and X_{mq_s} are the reactances that correspond to d- and q-axis magnetization reactances for a given air-gap flux and θ is the angle the air-gap flux makes with the d-axis. X_{mds} and X_{mq_s} are obtained from a given air-gap flux ψ_{ag} in the manner shown in Figure 4.2a. Shackshaft found from experiments that the reactances X_{md} and X_{mq} , for a flux in an intermediate axis, are related to X_i by the equations :

$$X_{md} = X_i + X_{sal} \sin^2 \theta \quad (4.8)$$

$$X_{mq} = X_i - X_{sal} \cos^2 \theta \quad (4.9)$$

where X_{sal} is an arbitrary constant. The variables of X_i , X_{md} and X_{mq} with the angle of the air-gap flux are shown in Figure 4.2b.

5.5 Effect of saturation of machine parameters on shaft torque.

The synchronous machine model described in Section 2.2 was modified by incorporating the model for leakage path and that for mutual path saturation as described in the previous section. The simulation of out-of-phase synchronization for different synchronizing angles was repeated considering the presence of machine saturation. In each case instantaneous values for stator current, electromagnetic air-gap torque, quill-shaft torque, coupling-shaft torque were calculated. From these values, maximum value of stator current and peak-to-peak value of

air-gap torque, and shaft torques were found and plotted for different synchronizing angles. These currents and torques including the effect of saturation were compared with those excluding saturation effect and the comparison is made in Figure 4.3, 4.4, 4.5 and 4.6 respectively.

Figure 4.3 shows the effect of saturation on maximum stator current following out-of-phase synchronization. It is found that when the saturation effect is included, the maximum value of stator current for a particular synchronizing angle is greater than that when the saturation effect is excluded. Since it is found [24] that by the effect of saturation the transient reactance reduces in magnitude as the magnitude of current increases, the increase in current during out-of-phase synchronization is thus obvious. For out-of-phase synchronization when the stator current increases, the machine saturates so the transient reactance reduces and hence the stator current becomes more and more until saturated value of the machine parameters are reached. This difference between currents with saturation included and that with saturation excluded is seen to be maximum at around 180 degree out-of-phase synchronization. This is because the stator current becomes greatest at around that particular synchronization angle. In our investigation the current during out-of-phase synchronization is found to be increased by 18 percent when the effect of saturation is considered.

Figure 4.4 shows the effect of saturation on peak-to-peak air-gap torque. Since electromagnetic air-gap torque is directly proportional to the stator current, it is also higher when saturation effect is considered. It is found that at an angle 180 degree the air-gap torque is 20 percent higher than that when there

is no saturation effects. Figures 4.5 and 4.6 show effect of saturation on peak-to-peak quill-shaft and coupling-shaft torque respectively. Since the shaft torques are developed as a result of air-gap torque, the quill-shaft and coupling-shaft torques are also higher when saturation effects are included in the model.

It is, therefore, concluded that machine saturation has a considerable effect on the responses during out-of-phase synchronization. So, the simulation of the phenomena must not neglect the saturation within the machine.

CHAPTER 5

**COMPARISON BETWEEN FAULTY SYNCHRONIZATION
AND SHORT CIRCUIT**

5.1 Introduction.

It has been stated in Chapter 1 that the shaft designers, in general, used to consider torques, developed during short circuit as the severe most case of disturbance. It is, therefore, necessary to investigate the effect of short circuit faults on shaft torques. The study should facilitate one to compare its effect with that developed during faulty synchronization. Previous studies [13] claimed that during short circuit, critical factor for maximum stress occurred just after the application of two-phase short circuit. While on fault clearance, critical factor became at the moment of clearing three-phase short circuit. Although high electromagnetic torques are experienced for two-phase faults on fault incidence, higher electromagnetic torques generally result on clearance of three-phase fault [2]. So torques developed due to three-phase short circuit has only been considered in the present investigation. For the sake of mathematical convenience, simultaneous interruption of currents in all three phases is assumed. The assumption does not make much difference in the results [29].

The generator and the shaft system was modelled as described in sections 2.2 and 2.3 respectively. The network configuration for the investigation of short circuit was very similar to that considered in the case of faulty synchronization. The synchronous generator supplied its power to an infinite bus-bar through the generator-transformer and a high voltage transmission line. The generator was considered to be operated at rated voltage and supplied rated output. Fault throwing tests were simulated by assuming a three-phase short circuit fault occurred suddenly on the line and was subsequently cleared. Simulation of these

fault throwing tests were carried out for different fault durations and different fault locations. In each case, time responses for stator current, electromagnetic air-gap torque, quill-shaft torque and coupling-shaft torque were calculated, analyzed and compared with those of faulty synchronization.

5.2 Simulation of fault throwing test.

The differential equations for a machine derived in Chapter 2 are used as the basis of simulation of three-phase short circuit fault occurrence and subsequent removal. Similar to simulation of faulty synchronization, the program for short circuit study starts with the measured values of initial steady-state condition prior to the application of short circuit. The relationship between the terminal quantities with five winding fluxes are used in order to determine the starting values of state space variables. As the fault is applied, the d- and q-axis components of terminal voltage are set equal to zero. The line resistance and reactance in between machine terminal and the fault point are added to the machine's resistances and reactances respectively. The step by step solution is carried out to calculate transient change in fluxes. The instantaneous fluxes are then used to calculate instantaneous currents. When the fault is removed, the d- and q-axis components of infinite bus-bar voltage are considered to be active as the remote end terminal voltage, but the total line resistance and reactance are added with the machine's resistances and reactances respectively. The time domain solution is then carried forward in time steps.

Machine 'A' was considered for the investigation of three-phase short circuit. The parameters of the machine are given in Table 1. Prior to application of

the three-phase fault, the generator was supplying rated power at rated voltage via its transformer of impedance, $Z_t = (0.0070 + 0.0704) \text{ pu}$ to a grid system of impedance, $Z_g s = (0.0002 + 0.0020) \text{ pu}$. A fault was created at the machine terminals and sustained for 70 milliseconds. It was then cleared and thus the machine was reconnected to the system. Therefore, two disturbances during the fault throwing test were occurred, one at the instant of fault application and the other at the moment of fault clearance. The transients of the electromechanical quantities were calculated using a computer program simulating the fault throwing test. The time responses showing stator current, air-gap torque, quill-shaft torque and coupling-shaft torque following a fault throwing test are shown in Figure 5.1. As found by others [2,13], it is observed that peak torque on fault clearance is much higher than that corresponding to fault incidence. It is also noticed that the air-gap torque decay rapidly whereas the shaft torques decay slowly. This is because of greater damping in electrical system in comparison to that in mechanical counterpart [13].

5.3 Effect of fault duration on peak-to-peak torque.

The time responses shown in Figure 5.1 were obtained for a fault duration of 70 milliseconds. Similar time responses for different fault duration, ranging from 50 to 150 millisecond in 5 millisecond increment were calculated using the program. The maximum value of stator current and the peak-to-peak values of air-gap torque, quill-shaft torque and coupling-shaft torque were found out from the time responses. The values are plotted against fault duration and the curves are shown in Figure 5.2.

Curve (i) shows that the peak stator current fluctuates cyclically as fault clearing time is varied. The frequency of this fluctuation is the same as the grid supply frequency of 50 Hz. Curve (ii) shows the peak-to-peak air-gap torque which also fluctuates cyclically with fault clearing time. The peak values depend on the moment, in the 50 Hz power cycle, at which the fault is cleared. This is why, the peaks are found to oscillate at a frequency of 50 Hz. The maximum values are found to occur when fault is cleared at the middle of the cycle, whereas the minimum values are occurred when fault is cleared at the beginning of the cycle.

Curve (iii) and (iv) show the variation of peak-to-peak quill-shaft and coupling-shaft torque respectively. Peak values of the shaft torques are determined by the superposition of two transient torques, one initiated at the fault incidence and other at the fault clearance. Each of the transient torques has power frequency, shaft oscillation frequency and unidirectional components [13]. The maximum of the peak values occur when all the components are in phase.

5.4 Effect of fault location on peak torque.

Turbine-generator shaft torque will vary if the location in the line at which the fault is occurred varies. In order to investigate the variations simulations of three-phase short circuit were carried out for different fault locations, keeping the fault duration fixed at 100 millisecond. The impedance between generator terminal and the infinite bus-bar is assumed to be composed of two sections, one between generator terminal and fault point and the other between fault point and the infinite bus. The location of fault was varied by varying the impedances of the two sections while keeping the total impedance fixed. This was done by

using a factor with the total impedance which is termed as location factor. When the value of the location factor is '0', it implies that the fault is occurred at the end of infinite bus, whereas if its value is 1, the fault is occurred at the generator terminal. Peak-to-peak value of torque during fault period and after fault clearance were extracted from the time responses for different fault locations. These peak-to-peak values of torque are plotted against location factor and shown in Figures 5.3 and 5.4.

Figure 5.3 shows the variation of peak-to-peak torques due to variation of fault location, during short circuit period. The curves demonstrate that during short circuit period if the location factor is increased i.e. the distance of fault from the generator is reduced, the electromagnetic air-gap torque is increased. Similarly quill-shaft and coupling-shaft torque are also increased. Figure 5.4 shows the variation of peak-to-peak torques due to change of fault location, after the fault is cleared. Similar variations are observed as found during short circuit period. Therefore, it can be concluded that for three-phase short circuit if the fault is occurred nearer to the generator, the developed torques become greater.

5.5 Comparison of faulty synchronization and short circuit.

During simulation of out-of-phase synchronization, discussed in Chapter 3, it has found that the amplitude of the shaft torques are maximum when the machine is synchronized at an angle of 128° , machine voltage leading busbar voltage. On the other hand, it has found during simulation of short circuit, discussed in the previous sections that the amplitude of the shaft torques are maximum during clearance of three-phase short circuit at the machine terminals with a fault

duration of 70 millisecond. To compare the amplitude of the electro-mechanical quantities during out-of-phase synchronization with those during short circuit, the maximum and peak-to-peak amplitude of torques as well as maximum amplitude of stator current are obtained for the two cases and shown in Table 2 and Table 3 respectively.

If the stator current during three-phase short circuit at the machine terminals is taken as the basis of comparison, then it is found that for the same stator current, the shaft torques developed during out-of-phase synchronization are much higher than that developed during short circuit. In our investigation it is found that in the case of a three-phase short circuit at the terminals, the maximum amplitude of current is found to be 17 pu when the peak-to-peak torque in the coupling-shaft is 9.5 pu. On the other hand, during out-of-phase synchronization, 17 pu current flows in the machine at synchronizing angle of 85° and 280° at which the peak-to-peak coupling-shaft torques are 13.5 pu and 11 pu respectively. Thus for the same value of current, the peak-to-peak amplitude of torques during out-of-phase synchronization are 1.42 and 1.15 times of those developed during a three-phase short circuit. The comparative study discussed above is shown in Table 4.

If the torque during three-phase short circuit at the machine terminals are taken as the basis of comparison, then it is found that for the same shaft torque the stator current during out-of-phase synchronization is smaller than that developed during short circuit. In our investigation it is found that in the case of a three-phase short circuit at the terminals, the peak-to-peak amplitude of coupling-

shaft torque is found to be 9.5 pu when the maximum amplitude of current is 17 pu. On the other hand it is found that 9.5 pu torque is developed during out-of-phase synchronization at angles 65° and 285° at which the maximum amplitude of currents are 11 pu and 15.5 pu respectively. Thus for the same value of torque, the maximum amplitude of stator currents during out-of-phase synchronization are 0.64 and 0.91 times of those flow during three-phase short circuit. The comparative study discussed above is shown in Table 5.

If the severe most cases in the two phenomenon are compared as given in Table 2 and Table 3, it is found that the maximum and peak-to-peak amplitude of the quill-shaft torque for out-of-phase synchronization are respectively 2.4 and 2.02 times of the torques developed during three-phase short circuit. Similarly the maximum and peak-to-peak amplitude of the coupling-shaft torque for out-of-phase synchronization are 2.6 and 2.05 times of the torques developed during three-phase short circuit. Thus it is clearly demonstrated that the shaft torques for out-of-phase synchronization is much greater than those developed during three-phase short circuit.

CHAPTER 6

CONCLUSION AND FURTHER WORK

6.1 Conclusion.

A comprehensive mathematical model for simulating faulty synchronization has been developed. The computer program written for the purpose has been used to study the different effects during the disturbance. The instantaneous variations of currents and torques following the faulty synchronization have been taken as the output of the program. The time responses were then studied. The peak variations of the machine responses for different synchronizing angles were obtained from the instantaneous responses. The effect of variations in different machine parameter and the variations in network parameters on the peak responses have also been studied. A simple expression for shaft torque due to faulty synchronization was developed representing the machine and the associated network by a simple equivalent circuits. The responses obtained from the computer simulation were explained with the help of the derived expressions. The analysis shows that the peak air-gap torque may occur at synchronizing angle of around 180° , whereas the peak values of quill- and coupling-shaft torque occur at two places, one at around 120° and other at around 240° .

The study has been repeated by incorporating saturation effect within the machine. This was done for the comparison of the responses with and without saturation. The Shackshaft's model [23] for mutual path saturation was taken into account for simulating saturation in the main flux path. On the other hand, the leakage path saturation model developed by Kabir et al [32] has been considered in the study. The effect of incorporating saturation model in the simulation of faulty synchronization was found to produce greater current and shaft torques than it would produce without

considering saturation. The study demonstrates that torques are increased by 10 to 20 percent for different synchronizing angles when saturation is properly taken into consideration.

In order to complete the study a comparison is made with responses obtained during a disturbance originated by three-phase short circuit fault. At first the current and torques developed due to short circuit fault was studied in detail. The effect of different parameters on the short circuit responses were also analyzed both at the initiation of fault and at the clearance of fault. And finally a comparative study is made between severe most cases during the two disturbances, namely, faulty synchronization and short circuit.

It can be concluded that the shaft design engineers should not, by any means, consider the short circuit torques as the basis of their design. Rather, the torques developed during faulty synchronization, especially at an angle of around 120 electrical degree should be thought as the maximum possible value of the developed torques. Of course, both mutual and leakage path saturation should be taken into account during calculation of peak values.

6.2 Further Work.

As the continuation of the work described, different area of further investigation may be considered. The important areas are :

- 1 . Although T.J. Hammons [13] in his investigation showed that the governor have insignificant effects on the responses, but how they behave when saturation of the machine is considered is not obvious from his study. Since the present study did

not consider the effect of governor for the simulation of faulty synchronization, so a rigorous analysis of the situation under saturated condition should be carried out including governor model.

- 2 . An approximate model for the simulation of faulty synchronization should be developed, so that multi-machine problems can be handled easily. The effect of faulty synchronization on the associated machines especially machines electrically nearer to the faulty one should be studied during the disturbance.
- 3 . The representation of lumped mechanical equivalence of shaft system is, sometimes, thought to be an approximate one. So, a study involving distributed mechanical analogous system may be carried out and the validity of approximate lumped model should thus be established.

REFERENCES

REFERENCES

- [1] ANSI C50.13-1977, American National Standard Requirements for Cylindrical Rotor Synchronous Generators published by IEEE, 1977.
- [2] M. Canay, "Stresses in Turbogenerator Sets Due to Electrical Disturbances", Brown Boveri Review, Vol. 62, No.9, 1975, pp. 435-443.
- [3] P. A. Rusche, Z. A. Katsiapis and D. M. Teiezenberg, "Turbine-generator Shaft Related System Planning Criteria, Operating Experiences and Selected Study Results", IEEE Transaction on Power Apparatus and Systems, Vol PAS-99, No.6 Nov./Dec. 1980, pp 2153-2163.
- [4] P. A. Rusche, "Preliminary Results of an Investigation in to the Torsional Shaft Failure of a 21 MW Combustion Turbines", Joint Power Generation Conference, Buffalo, N.Y., September 1976, pp 19-23.
- [5] A. S. Aldred, "Electronic Analogue Computer Simulation of Multimachine Power System Network", IEE Proceedings Vol. 109A, No. 45, June 1962. pp 195-202.
- [6] B. D. Nellist and S. M. El-Sobki, "Recent Imporvements in Transformer Analogue Networks", IEE Proceedings, Vol. 110, No.7, 1963.
- [7] A. J. Wood, "Synchronizing Out of Phase", AIEE Transactions, April 1957, pp 1-10.
- [8] C. Concordia, "Synchronous Machines", a book published by Wiley,1951.

- [9] R. H. Park, "Two-Reaction Theory of Synchronous Machines, General Method of Analysis, Part-1", AIEE Transactions, Vol. 48, 1929, pp 716-730.
- [10] P. C. Krause, W. C. Hollopeter, D. M. Triesenberg and P. A. Rusche, "Shaft Torque During Out of Phase Synchronization", IEEE Transactions on Power Apparatus and Systems, Vol. PAS-96, No.4, July/August 1977, pp 1318-1323.
- [11] J. V. Mitsche, P. A. Rusche, "Shaft Torsional Stress due to Asynchronous Faulty Synchronization", IEEE Transactions on Power Apparatus and Systems, Vol. PAS-99, No. 5, Sept/Oct 1980. pp 1864-1870.
- [12] T. J. Hammons, "Stressing of Large Turbo-Generators at Shaft Coupling and LP Turbine Final-Stage Blade Roots following clearance of Grid System and Faulty Synchronization", IEEE Transactions on Power Apparatus and Systems, Vol. PAS-99, No.4, July/Aug 1980 pp 1652-1662.
- [13] T. J. Hammons, "Effect of Three Phase System Faults and Faulty Synchronization on the Mechanical Stressing of Large Turbo-Generators", Revue Generate de l'Electricite, July-August 1977, Vol. 86 No. 7/8, pp 558-580.
- [14] T. J. Hammons, "Effect of Damper Modelling and the Fault Clearing Process on Response Torque and Stressing of Turbine-Generator Shafts", IEEE Transactions on Energy Conversion, Vol. EC-1, No.1, March 1986. pp 113-121.
- [15] IEEE Committee Report, "Computer Representation of Excitation Systems", IEEE Transactions on Power Apparatus and Systems, Vol. PAS-87, 1968, pp 1460-1464.

- [16] R. H. Park, "Two-Reaction Theory of Synchronous Machines, Part-II", AIEE Transactions, Vol. 52, 1933, p 52.
- [17] Y. Takeda and B. Adkins, "Determination of Synchronous Machine Parameters Allowing for Unequal Mutual Inductances, IEE Proceedings, Vol. 121, No.11, Nov. 1974, pp 1501-1504.
- [18] G. Shackshaft, "New Approach to the Determination of Synchronous Machine Parameters from Tests", IEE Proceedings, No. 121, No.11, Nov. 1974, pp 1385-1392.
- [19] I. M. Canay, "Causes of Discrepancies on Calculation of Rotor Quantities and Exact Equivalent Diagrams of Synchronous Machines", IEEE Transactions on Power Apparatus and Systems, Vol. PAS-88, No.7, July 1969, pp 1114-1120.
- [20] S. M. L. Kabir, "Digital Modelling of Large Alternator", a Ph.D. thesis, University of Manchester, 1989.
- [21] R. G. Harley, D. J. N. Limerbear and E. Chirrieozzi, "Comparative Study of Saturation Methods in Synchronous Machine Models", IEE Proceedings, Vol. 127, Part B, No. 1, January 1980, pp 759-763.
- [22] L. Salvatore, "Experimental Determination of Synchronous Machine Parameters", IEE Proceedings, Vol. 128, Part B, No.4, July 1981, pp 212-218.
- [23] G. Shackshaft, "Model of Generator Saturation for use in Power System Studies", IEE Proceedings, Vol. 126, No. 8, August 1979, pp 759-763.
- [24] L. A. Kilgore, "Effect of Saturation on Machine Reactances", AIEE Transactions, May 1935, pp 545-550.

- [25] C. Concordia, "Synchronous Machines", Volume 3", a book published by John Wiley, Newyork, 1951.
- [26] D. C. Macdonald, A. B. J. Reece and P. J. Turner, "Turbine Generator Steady-State Reactances", IEE Proceedings, Vol. 132, Part C, No. 3, May 1985, pp 101-108.
- [27] J. C. Flores, G. W. Buclay and McPherson Jr., "The Effect of Saturation on the Armature Leakage Reactance of Large Synchronous Machines", IEEE Transactions on Power Apparatus and Systems, Vol. PAS-103, No. 3, March 1984.
- [28] P. J. Turner and D. C. Macdonald, "Transient Electromagnetic Analysis of Turbine Generator Flux Decay Test", IEEE Transactions on Power Apparatus and Systems, Vol. PAS-101, No.9, September 1982, pp 3193-3199.
- [29] B. Adkins and R. G. Harely, "A General Theory of Alternating Current Machines", a book published by Chapman and Hall, London, 1975.
- [30] I. M. Canay, H. J. Rohrer and K. E. Schnirel, "Effect of Electrical Disturbances, Grid Recovery Voltage and Generator inertia on maximization of Mechanical Torques in Large Turbogenerator Sets", IEEE Transactions on Power Apparatus and Systems, Vol. PAS-99, No.4, July/Aug. 1980. pp 1357-1370.
- [31] M. Canay, "Stress in Turbogenerator Sets due to Electrical Disturbances", Brown Boveri Review, 1975(9), p 435-443.
- [32] S. M. Lutful Kabir and M. Mujibur Rahman, "Incorporation of Leakage Path Saturation in Synchronous Generator Model", Electric Machine and Power Systems, Vol. 21, No.3, (to be published).

APPENDICES

Appendix A

The Elements of Matrices in Equation 2.12

The elements of $A[5 \times 5]$, $A[5]$, $F[5]$ and $B[1]$ matrices of equation (2.12) are expressed as follows :

$$A(1,1) = [c_1 R_f Y_d(2,1) + c_2 R_{kd} Y_d(3,1) + c_3 Y_d(1,1)] / c_0$$

$$A(1,2) = [c_1 R_f Y_d(2,2) + c_2 R_{kd} Y_d(3,2) + c_3 Y_d(1,2)] / c_0$$

$$A(1,3) = [c_1 R_f Y_d(2,3) + c_2 R_{kd} Y_d(3,3) + c_3 Y_d(1,3)] / c_0$$

$$A(1,4) = [-1 - XY_g(1,1)] / c_0$$

$$A(1,5) = [-XY_g(1,2)] / c_0$$

$$A(2,1) = -R_f Y_d(2,1)$$

$$A(2,2) = -R_f Y_d(2,2)$$

$$A(2,3) = -R_f Y_d(2,3)$$

$$A(3,1) = -R_{kd} Y_d(3,1)$$

$$A(3,2) = -R_{kd} Y_d(3,2)$$

$$A(3,3) = -R_{kd} Y_d(3,3)$$

$$A(4,1) = [1 + XY_d(1,1)] / c_0$$

$$A(4,2) = XY_d(1,2) / c_0$$

$$A(4,3) = XY_d(1,3) / c_0$$

$$A(4,4) = [d_1 R_{kq} Y_q(2,1) + d_2 Y_q(1,1)] / d_0$$

$$A(4,5) = [d_1 R_{kq} Y_q(2,2) + d_2 Y_q(1,2)] / d_0$$

$$A(5,4) = - R_{kq} Y_q(2,1)$$

$$A(5,5) = - R_{kq} Y_q(2,2)$$

$$F(1) = [\{ XY_q(1,1) \omega_0 \psi_q + \omega_0 \psi_q + XY_q(1,2) \omega_0 \psi_{kq} \} \delta + \omega_0 V_{bd}] / c_0$$

$$F(4) = [\{ XY_d(1,1) \omega_0 \psi_q + \omega_0 \psi_q + XY_d(1,2) \omega_0 \psi_f + XY_d(1,3) \omega_0 \psi_{kd} \} \delta - \omega_0 V_{bq}] / c_0$$

$$B(1) = - \omega_0 c_1 / c_0$$

$$B(2) = \omega_0$$

$$\text{Where, } c_0 = 1 + XY_d(1,1)$$

$$c_1 = XY_d(1,2)$$

$$c_2 = XY_d(1,3)$$

$$c_3 = - (R + R_a)$$

$$d_0 = 1 + XY_q(1,1)$$

$$d_1 = XY_q(1,1)$$

$$d_2 = c_3$$

The elements not mentioned above are all equal to zero.

Appendix B

Elaborate Form of Model for Mechanical System

The state space model for the mechanical system :

$$\begin{bmatrix} \dot{\delta}_1 \\ \dot{\delta}_2 \\ \dot{\delta}_3 \\ \ddot{\delta}_1 \\ \ddot{\delta}_2 \\ \ddot{\delta}_3 \end{bmatrix} = \begin{bmatrix} 0 & 0 & 0 & 1 & 0 & 0 \\ 0 & 0 & 0 & 0 & 1 & 0 \\ 0 & 0 & 0 & 0 & 0 & 1 \\ -\frac{K_1}{J_1} & \frac{K_1}{J_1} & 0 & 0 & 0 & 0 \\ \frac{K_1}{J_2} & -\frac{K_1+K_2}{J_2} & \frac{K_2}{J_2} & 0 & 0 & 0 \\ 0 & \frac{K_2}{J_3} & -\frac{K_2+K_3}{J_3} & 0 & 0 & 0 \end{bmatrix} \begin{bmatrix} \delta_1 \\ \delta_2 \\ \delta_3 \\ \dot{\delta}_1 \\ \dot{\delta}_2 \\ \dot{\delta}_3 \end{bmatrix} + \begin{bmatrix} 0 \\ 0 \\ 0 \\ \frac{T_m}{J_1} \\ 0 \\ -\frac{T_m}{J_3} \end{bmatrix}$$

Appendix C

Time Domain Solution of Shaft Torque

The equation for Laplace transform of shaft torque is given by :

$$T_s(s) = \frac{2|V|^2 K_c}{|X|J_e} \frac{\omega m \cos \theta + sm \sin \theta}{(s^2 + \omega^2) \left(s^2 + \frac{4K_c}{J_e} \right)} \quad (\text{C.1})$$

Let us suppose, the expression be expressed in partial fraction as :

$$\frac{2|V|^2 K_c}{|X|J_e} \frac{\omega m \cos \theta + sm \sin \theta}{(s^2 + \omega^2) \left(s^2 + \frac{4K_c}{J_e} \right)} = \frac{As + B}{s^2 + \omega^2} + \frac{Cs + D}{s^2 + \frac{4K_c}{J_e}} \quad (\text{C.2})$$

Multiplying both sides with $(s^2 + \omega^2) \left(s^2 + \frac{4K_c}{J_e} \right)$ we have,

$$\frac{2|V|^2 K_c}{|X|J_e} (\omega m \cos \theta + sm \sin \theta) = (As + B) \left(s^2 + \frac{4K_c}{J_e} \right) + (Cs + D)(s^2 + \omega^2) \quad (\text{C.3})$$

Now equating the coefficients of s^3 , s^2 , s and constants we have,

$$A = -C \quad (\text{C.4})$$

$$B = -D \quad (\text{C.5})$$

$$\frac{2|V|^2 K_c}{|X|J_e} m \sin \theta = \frac{4AK_c}{J_e} + C\omega^2 \quad (\text{C.6})$$

$$\frac{2|V|^2 K_c}{|X|J_e} \omega m \cos \theta = \frac{4BK_c}{J_e} + D\omega^2 \quad (\text{C.7})$$

From equation (C.4) and (C.6),

$$\begin{aligned}\frac{2|V|^2 K_c}{|X|J_e} m \sin \theta &= \frac{4AK_c}{J_e} - A\omega^2 \\ \text{or, } A &= \frac{2|V|^2 K_c}{|X|J_e} \frac{m \sin \theta}{\left(\frac{4AK_c}{J_e} - \omega^2\right)} \\ \text{or, } A &= Km \sin \theta\end{aligned}\quad (\text{C.8})$$

$$\text{where, } K = \frac{2|V|^2 K_c}{|X|J_e \left(\frac{4AK_c}{J_e} - \omega^2\right)}$$

$$\text{Therefore, } C = -Km \sin \theta \quad (\text{C.9})$$

From equation (C.5) and (C.7),

$$\begin{aligned}\frac{2|V|^2 K_c}{|X|J_e} \omega m \cos \theta &= \frac{4BK_c}{J_e} - B\omega^2 \\ \text{or, } B &= \frac{2|V|^2 K_c}{|X|J_e} \frac{\omega m \cos \theta}{\left(\frac{4BK_c}{J_e} - \omega^2\right)} \\ \text{or, } B &= K\omega m \cos \theta\end{aligned}\quad (\text{C.10})$$

$$\text{Therefore, } D = -K\omega m \cos \theta \quad (\text{C.11})$$

Putting the values of A, B, C, and D in equation (C.2) we have,

$$\begin{aligned}T_s(s) &= \frac{Ksm \sin \theta + K\omega m \cos \theta}{s^2 + \omega^2} - \frac{Ksm \sin \theta + K\omega m \cos \theta}{\left(s^2 + \frac{4K_c}{J_e}\right)} \\ &= Km \sin \theta \frac{s}{s^2 + \omega^2} + Km \cos \theta \frac{\omega}{s^2 + \omega^2} \\ &\quad - Km \sin \theta \frac{s}{s^2 + \omega_m^2} - Km \cos \theta \frac{\omega \omega_m}{\omega_m (s^2 + \omega_m^2)}\end{aligned}\quad (\text{C.12})$$

where, $\omega_m = \sqrt{\frac{4K_s}{J_s}}$ is the natural frequency of the mechanical system oscillation. Now, inverting $T_s(s)$ the time domain solution is:

$$\begin{aligned}
 T_s(t) &= Km \sin \theta \cos \omega t + Km \cos \theta \sin \omega t \\
 &\quad - Km \sin \theta \cos \omega_m t - Km \frac{\omega}{\omega_m} \cos \theta \sin \omega_m t \\
 &= Km \sin(\omega t + \theta) \\
 &\quad - Km \sin \theta \cos \omega_m t - Km \frac{\omega}{\omega_m} \cos \theta \sin \omega_m t \tag{C.13}
 \end{aligned}$$

TABLES

Table 1

Comparative study between two sets of machine parameters

Parameters	Machine A	Machine B
Rating(MVA)	20.65	777.00
X_d (pu)	1.45	1.78
X'_d (pu)	0.131	0.271
X''_d (pu)	0.088	0.223
X_q (pu)	1.36	1.69
X''_q (pu)	0.088	0.222
T'_d (sec)	0.533	1.14
T''_d (sec)	0.0122	0.0265
T''_q (sec)	0.00323	0.0265
R_a (pu)	0.00466	0.00227
X_a (pu)	0.075	0.212
H (kWs/kVA)	2.238	3.197

Table 2

Torques and current following out-of-phase synchronization of 128 degree

	Maximum Amplitude in pu	Peak to Peak Amplitude in pu
T_e	29.0	35.0
T_q	12.0	17.0
T_c	13.0	19.5
I_a	29.0	-

Table 3

Torques and current following a three phase short-circuit at the machine terminals

	Maximum Amplitude in pu	Peak-to-Peak Amplitude in pu
T_e	11.0	18.0
T_q	5.0	8.4
T_c	5.0	9.5
I_a	17.0	-

Table 4

Comparison of shaft torques for the same value of stator current

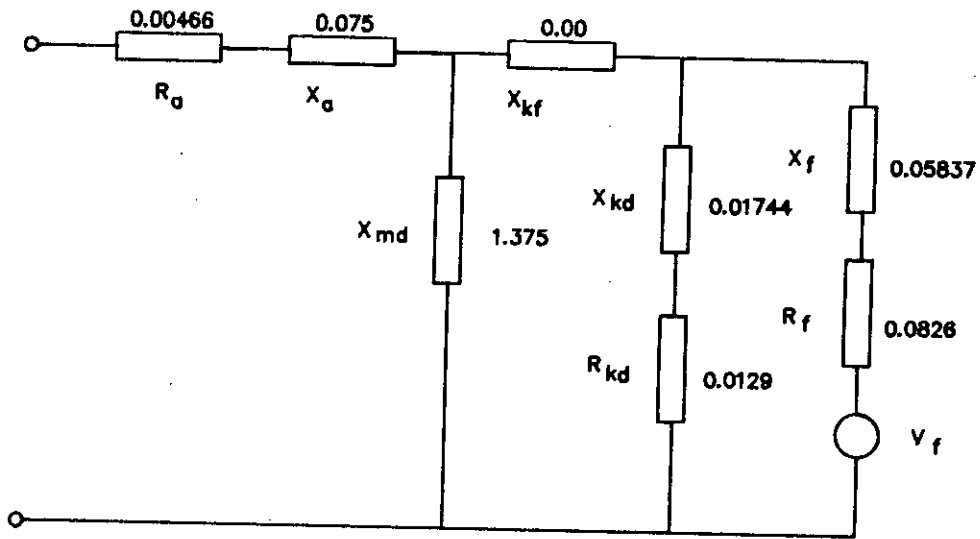
During Short current		During out-of-phase synchro.		
Torque in pu	Current in pu	Current in pu	Syn. angle in degree	Torque in pu
9.5	17	17	85°	13.5
			280°	11.0

Table 5

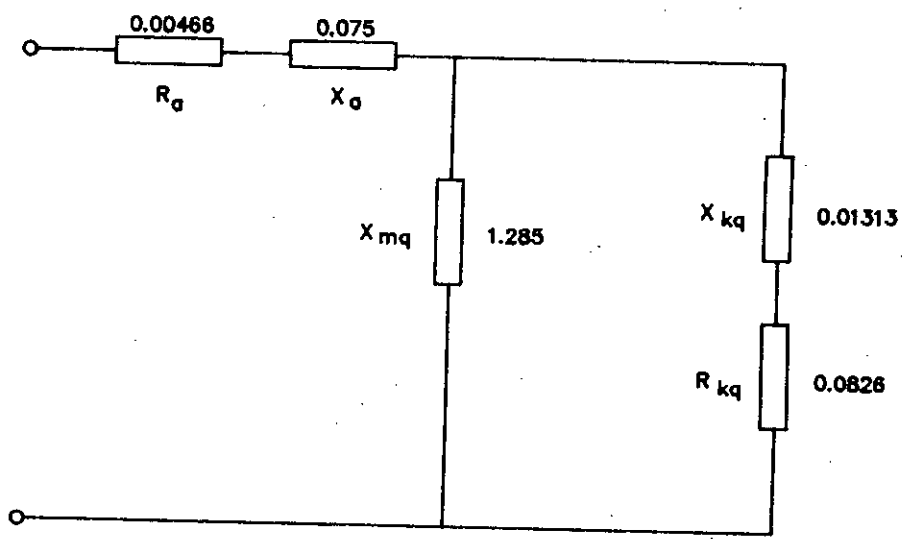
Comparison of stator current for the same value of shaft torque

During Short current		During out-of-phase synchro.		
Current in pu	Torque in pu	Torque in pu	Syn. angle in degree	Current in pu
17	9.5	9.5	65°	11.0
			285°	15.5

FIGURES



a) Direct axis



b) Quadrature axis

Fig 2.1 : The equivalent circuit of synchronous machine

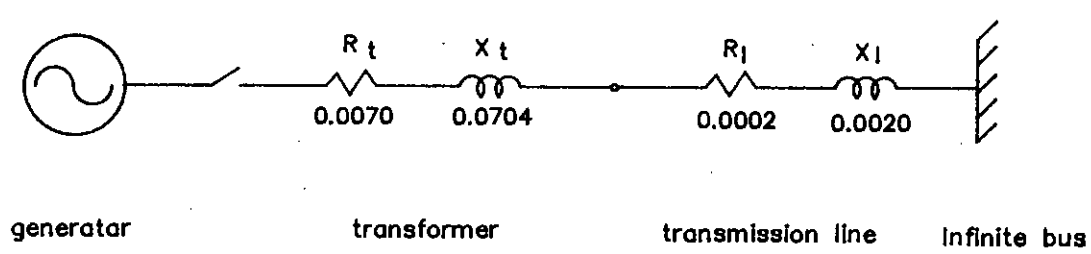
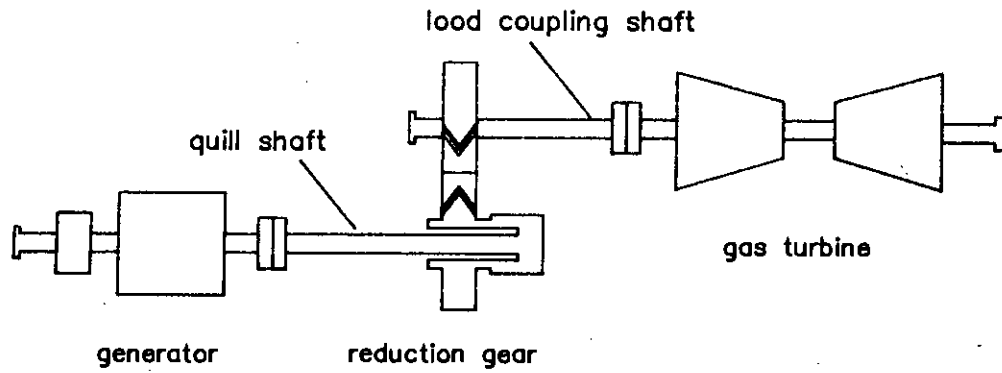
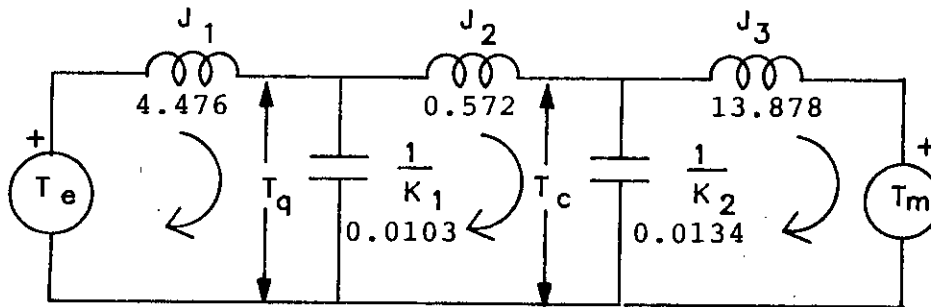


Fig 2.2 : Electrical network for the system studied



a) Block Diagram.



b) Analogous Circuit

Fig 2.3 : Representation of shaft assembly

85685

63

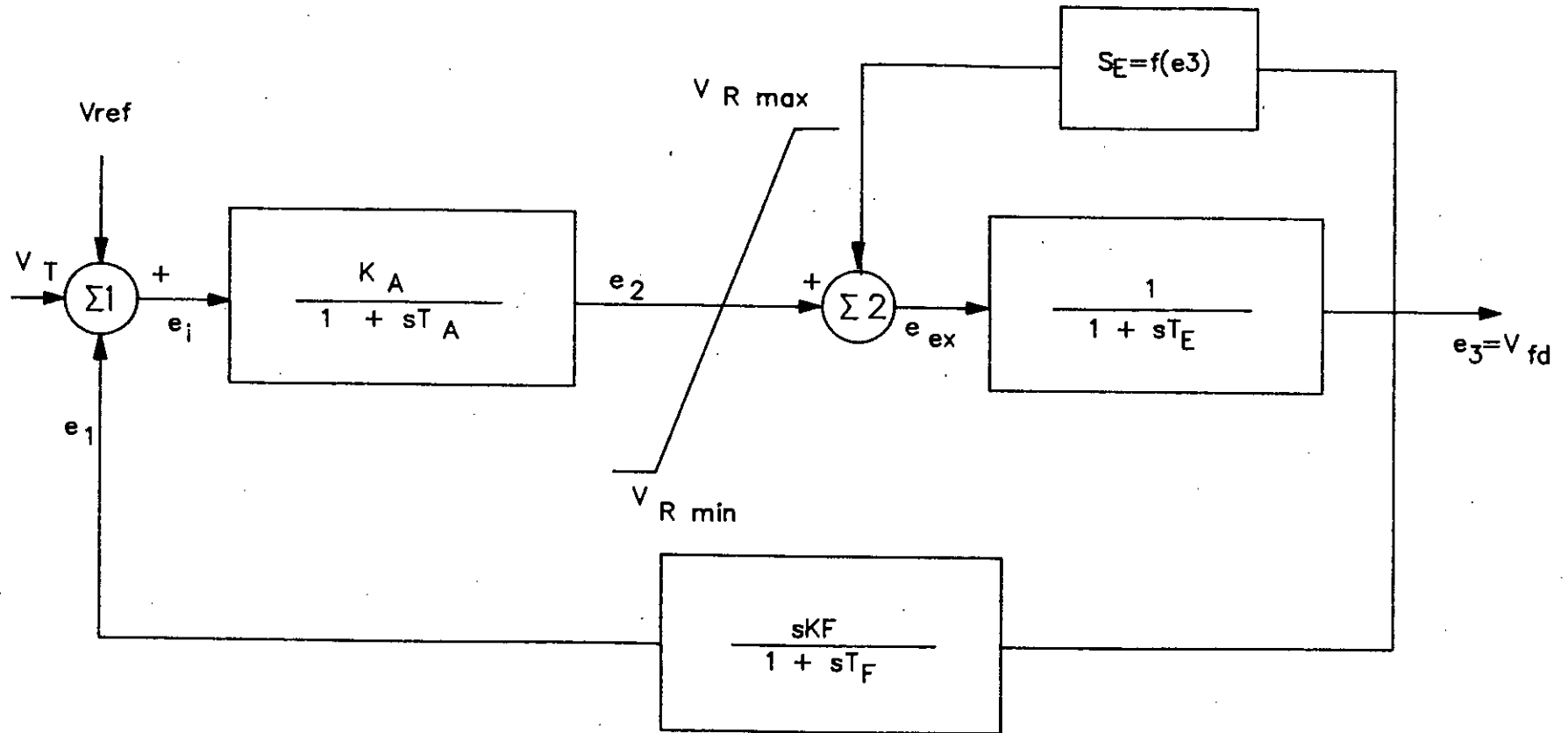


Fig 2.4 : Block diagram of an Automatic Voltage Regulator

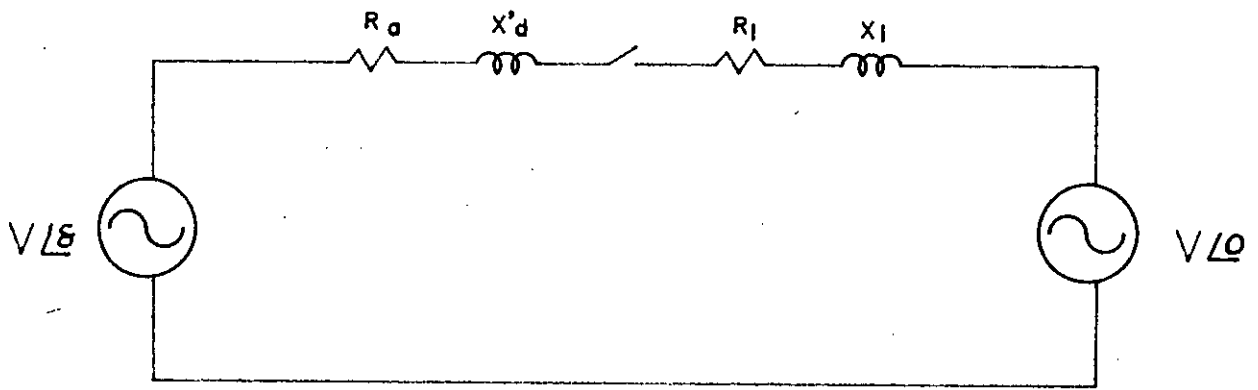


Fig 3.1 : Approximate representation of the electrical system

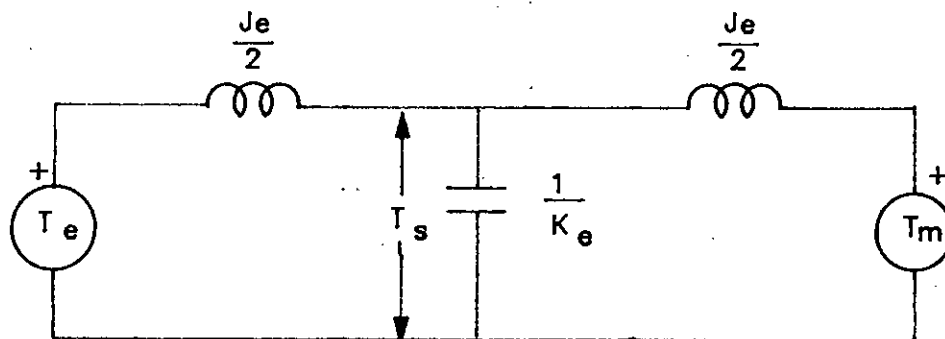


Fig 3.2 : T-section equivalent circuit of the turbine-generator shaft system.

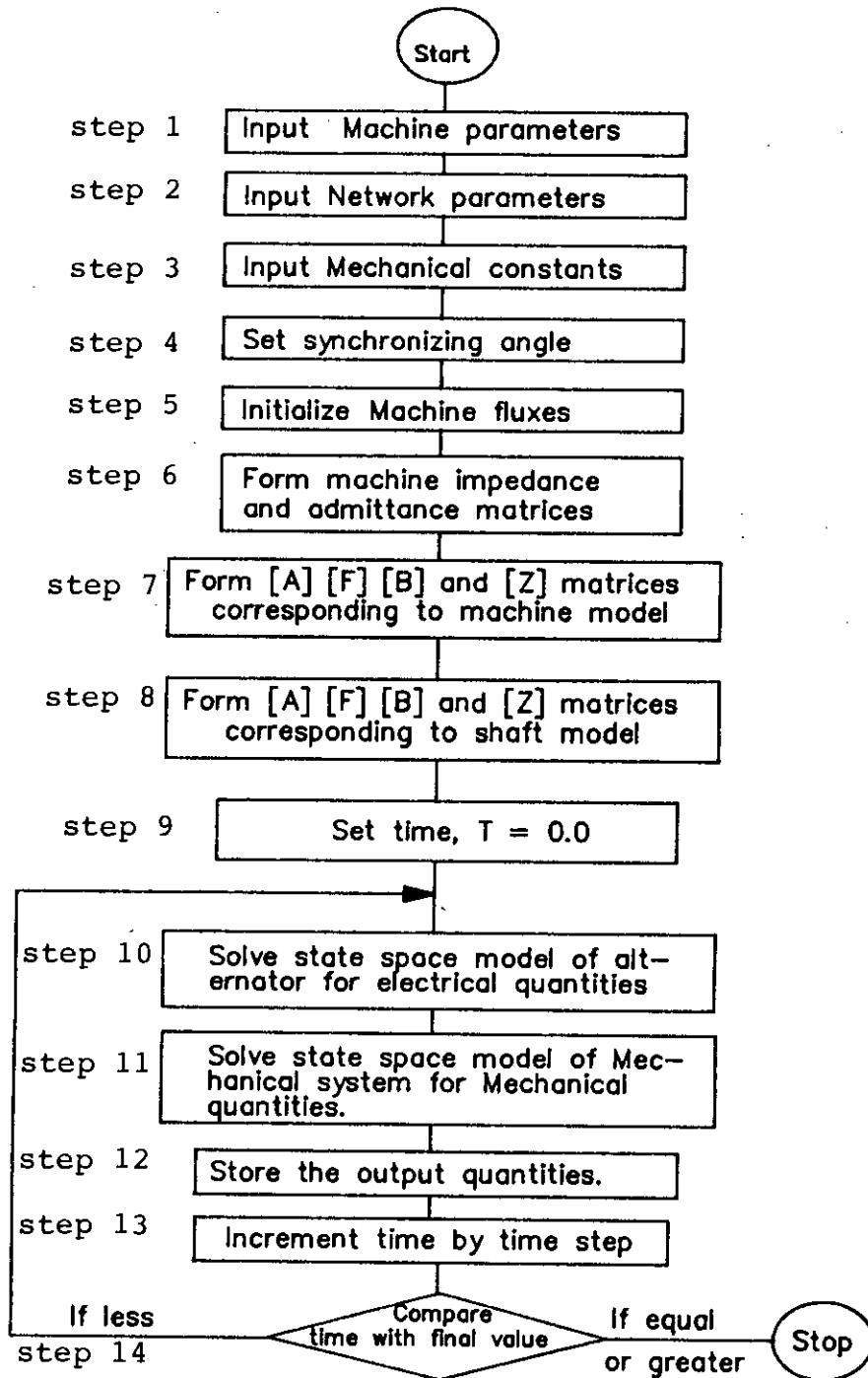


Fig 3.3 : Flow diagram of the computer program for study on faulty synchronization.

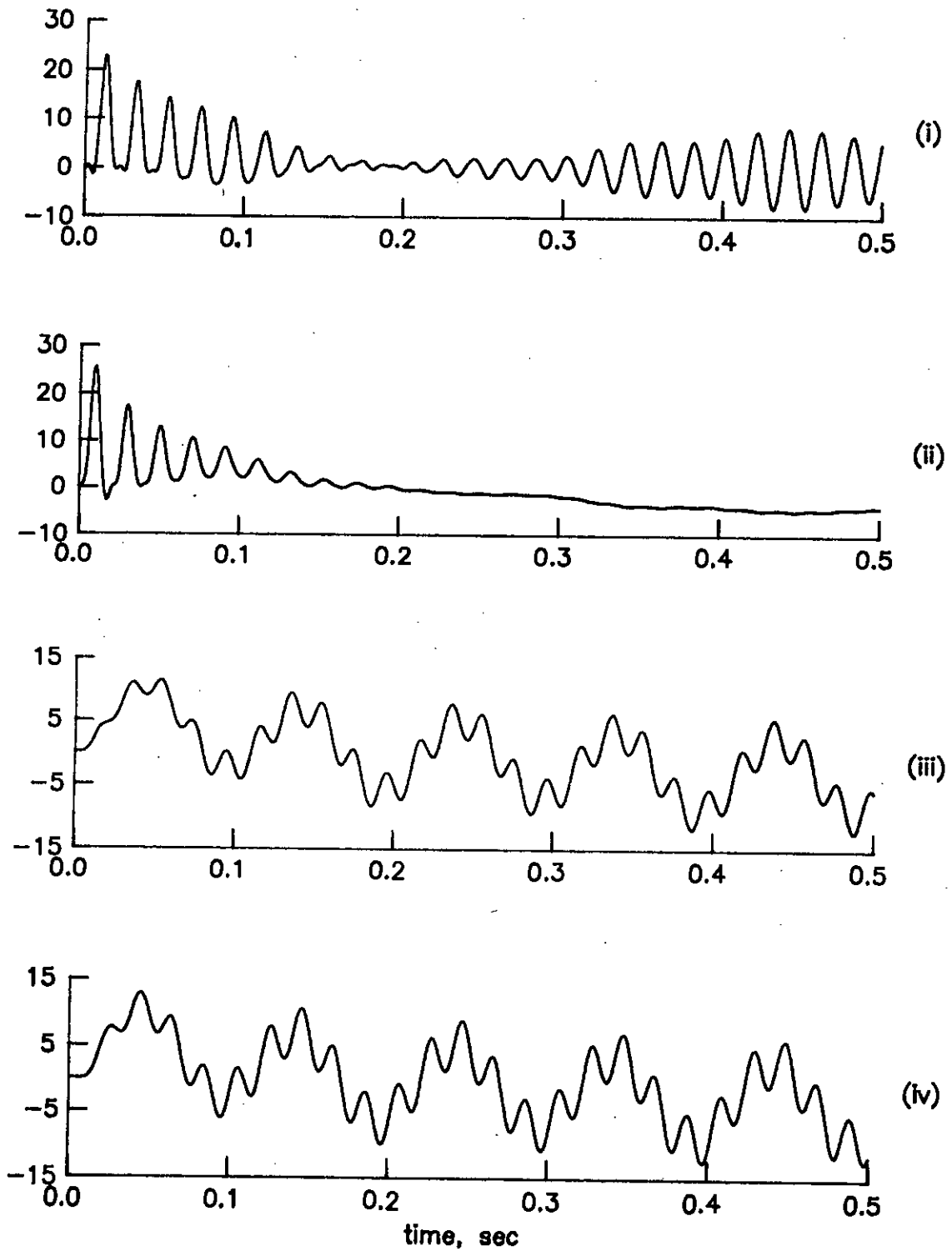


Fig 3.4 : Time response of machine 'A' during out of phase synchronisation of 120 degree, machine voltage leading transformer voltage.

(i) stator current, pu (iii) quill shaft torque, pu
(ii) airgap torque, pu (iv) coupling shaft torque, pu

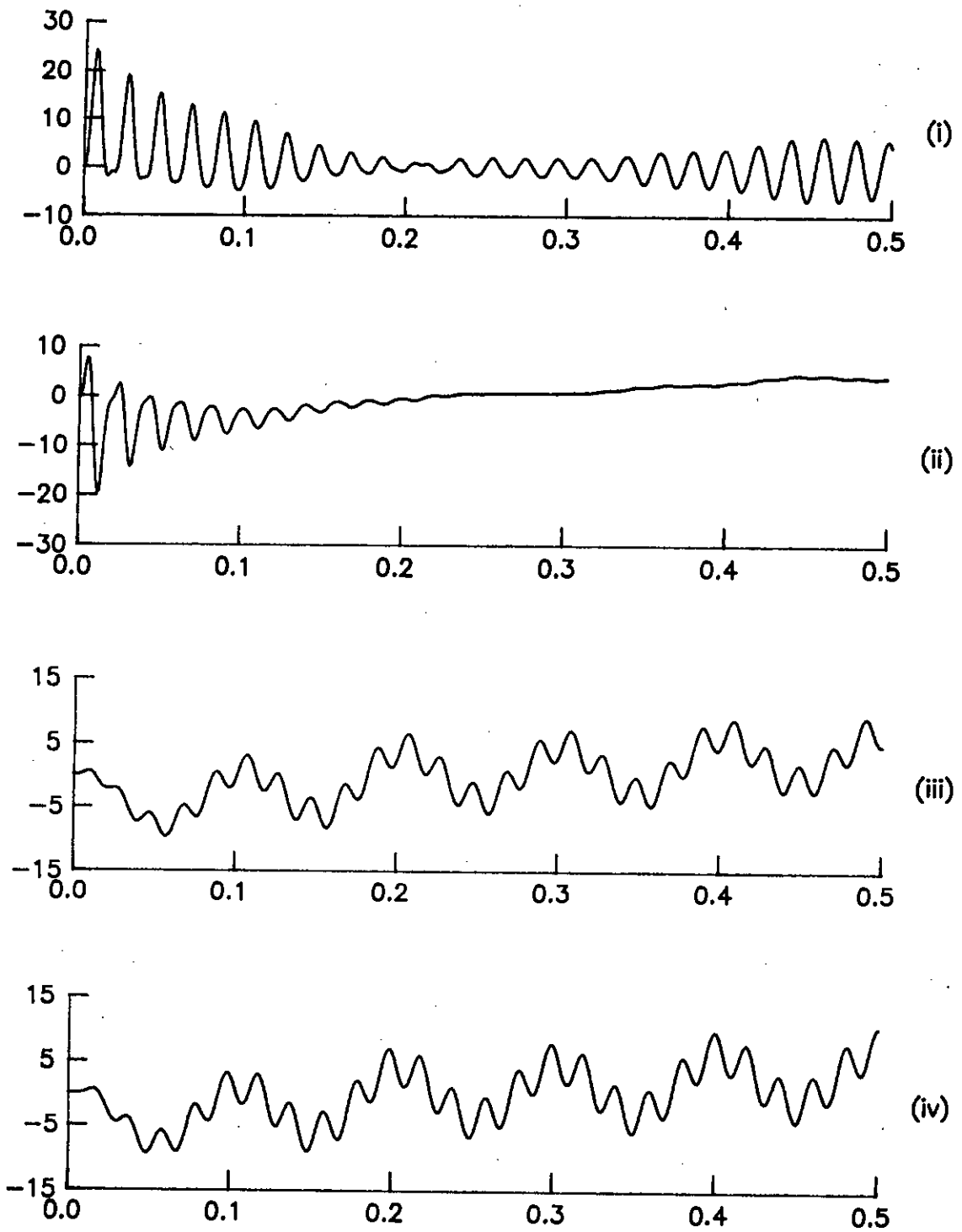


Fig 3.5 : Time response of machine 'A' during out of phase synchronization of 120 degree, machine voltage lagging transformer voltage.

(i) stator current, pu (iii) quill shaft torque, pu
(ii) airgap torque, pu (iv) coupling shaft torque, pu

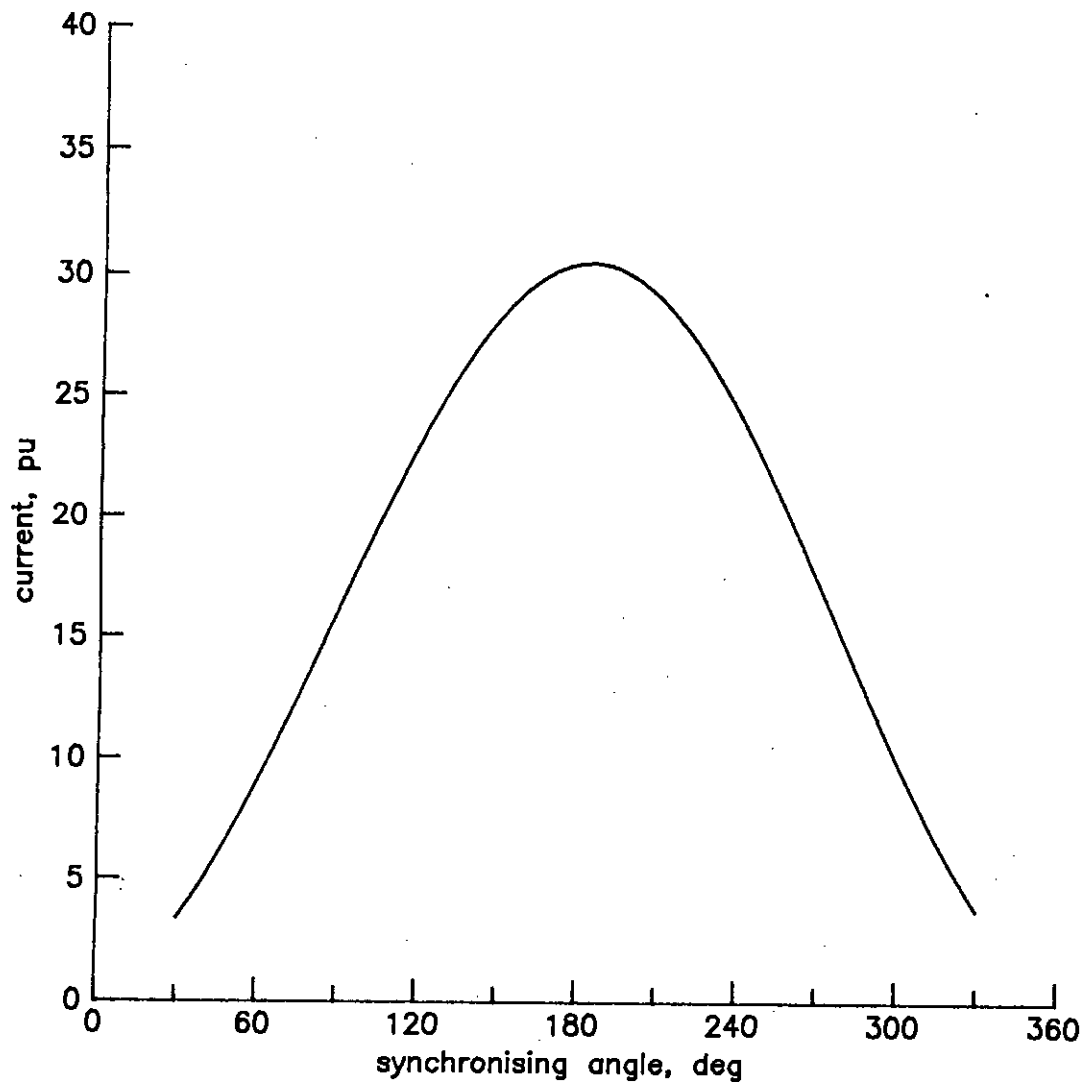


Fig 3.6 : Maximum current following out of phase synchronisation for machine 'A'.

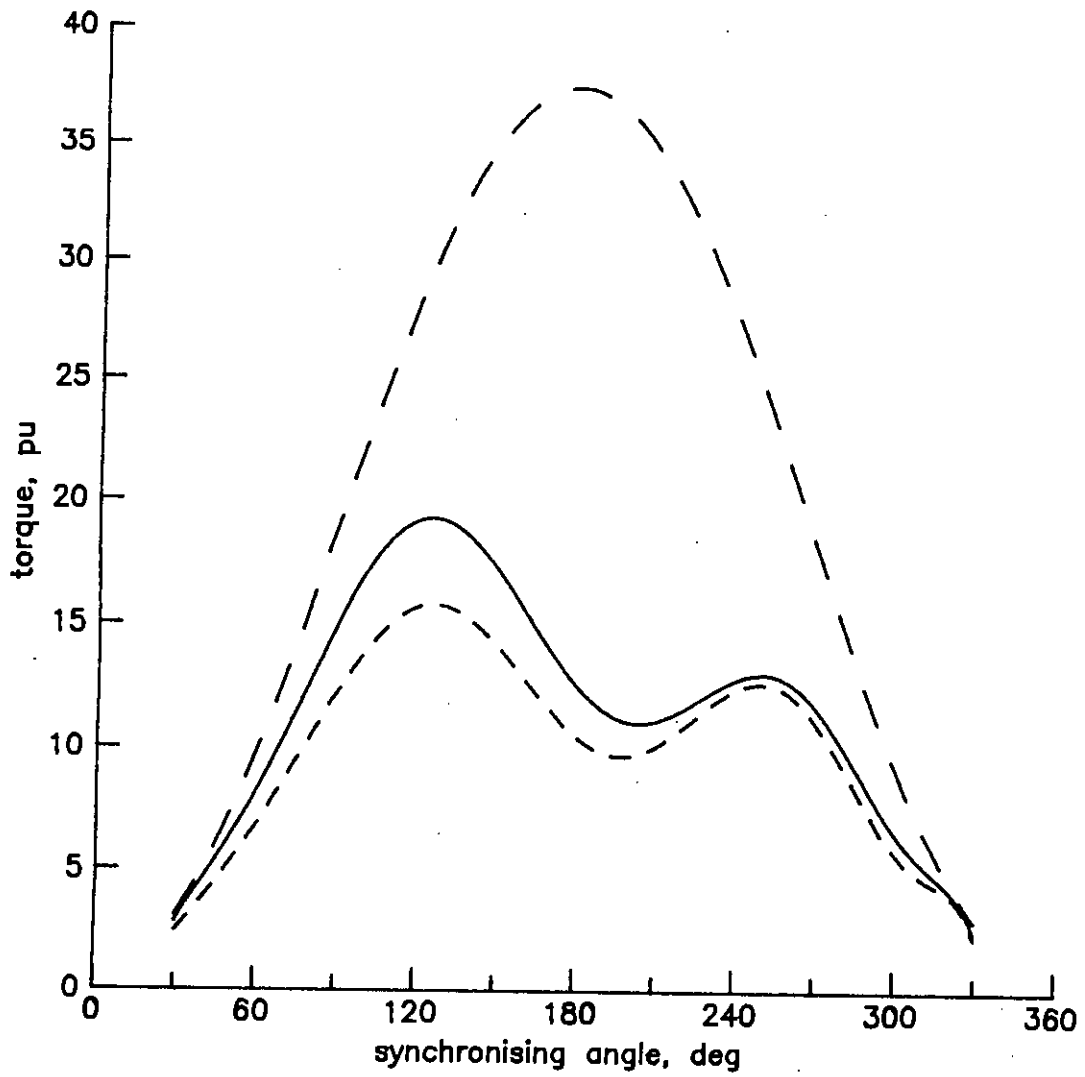


Fig 3.7 : Peak to peak shaft torque following out of phase synchronisation for machine 'A'.

- — — air gap torque
- - - quill shaft torque
- coupling shaft torque

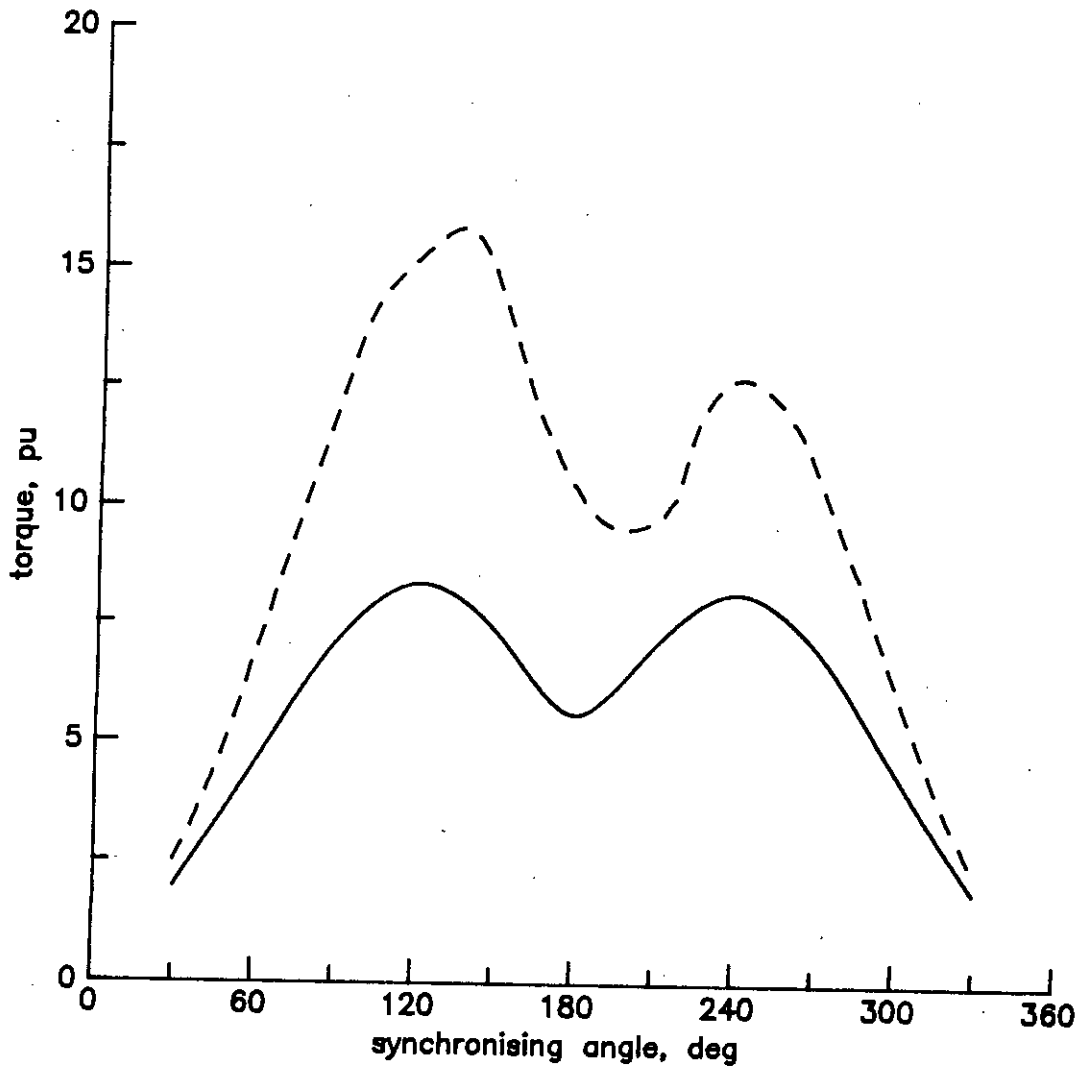


Fig 3.8: Effect of machine parameter on peak to peak quill shaft torque following out of phase synchronisation.

--- machine 'A'
 — machine 'B'

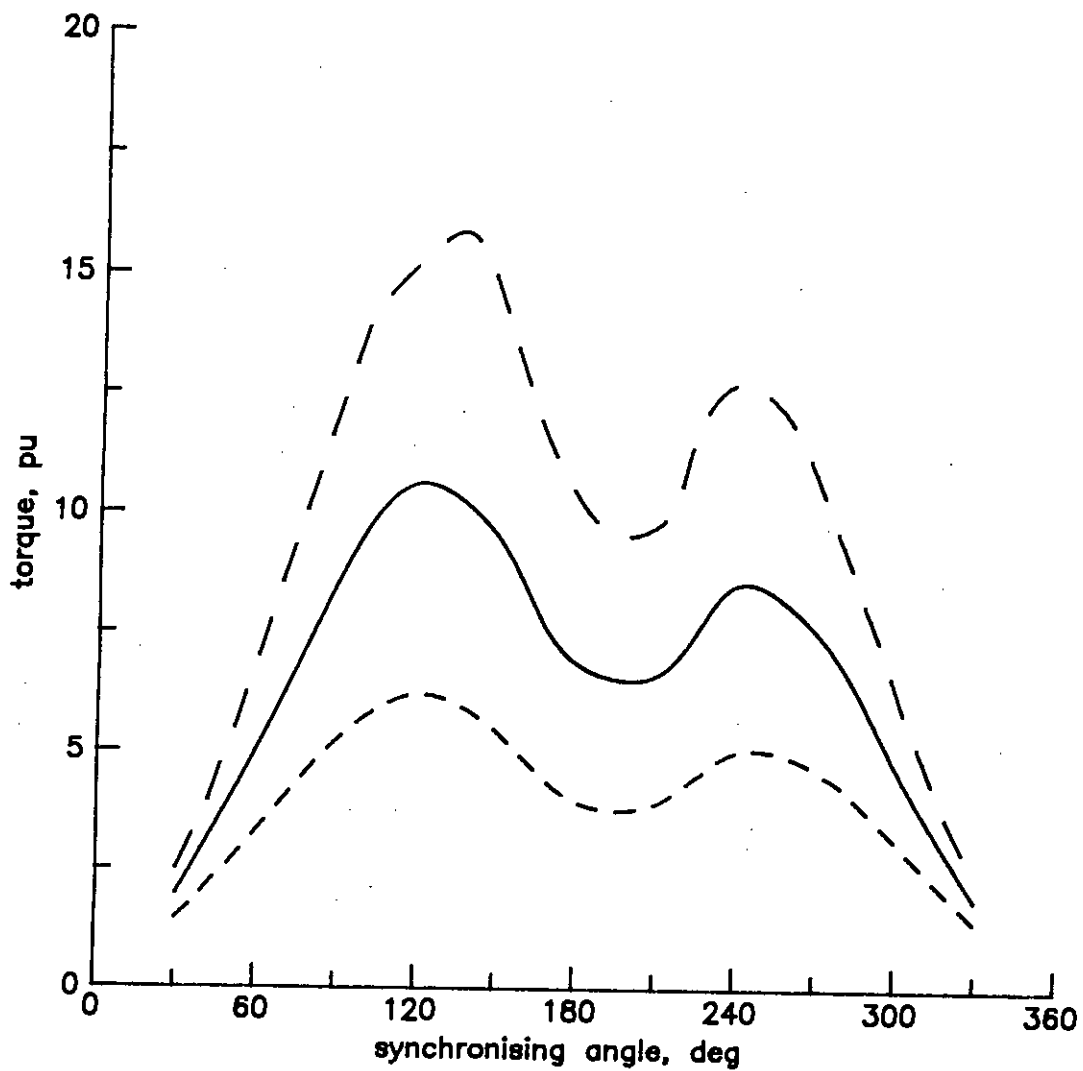


Fig 3.9 : Effect of network parameter on peak to peak quill shaft torque following out of phase synchronisation.

- - - RL=0.0072 pu , XL=0.0724 pu
 ——— RL=0.0144 pu , XL=0.1448 pu
 - . - RL=0.0288 pu , XL=0.2896 pu

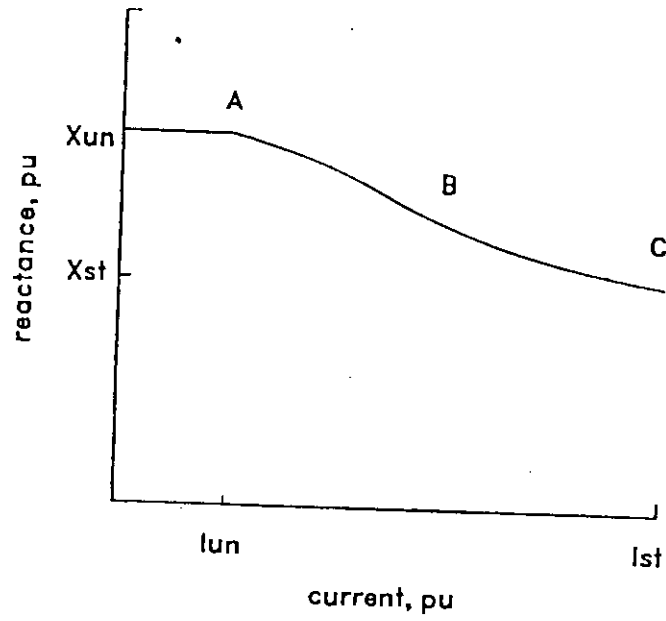


Fig 4.1 : Leakage path saturation characteristics

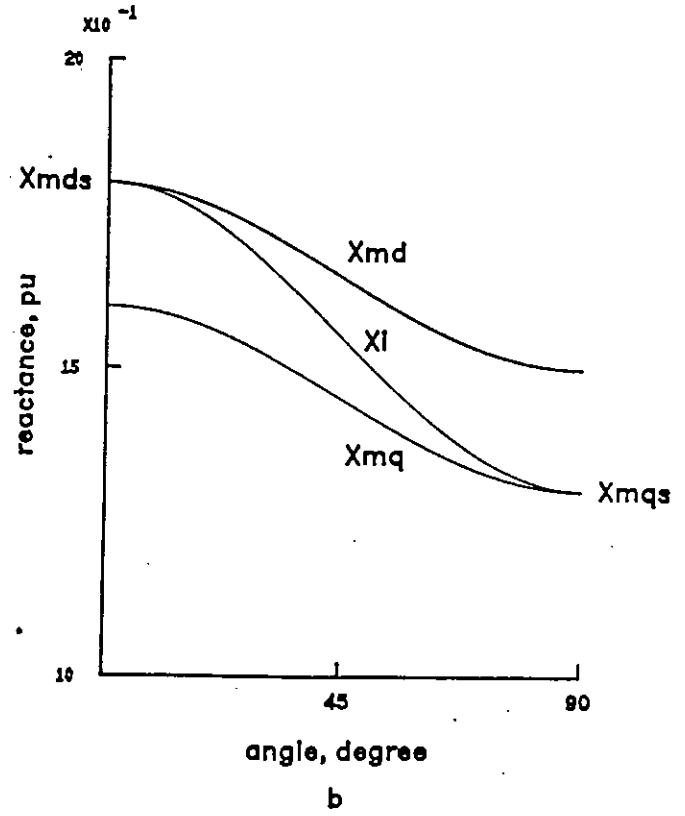
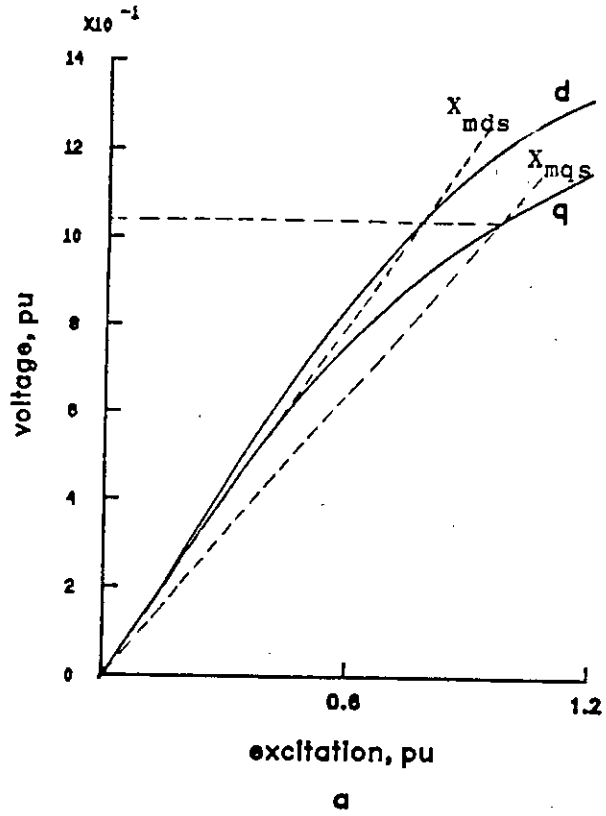


Fig 4.2 : Shackshaft's method of calculating mutual reactances

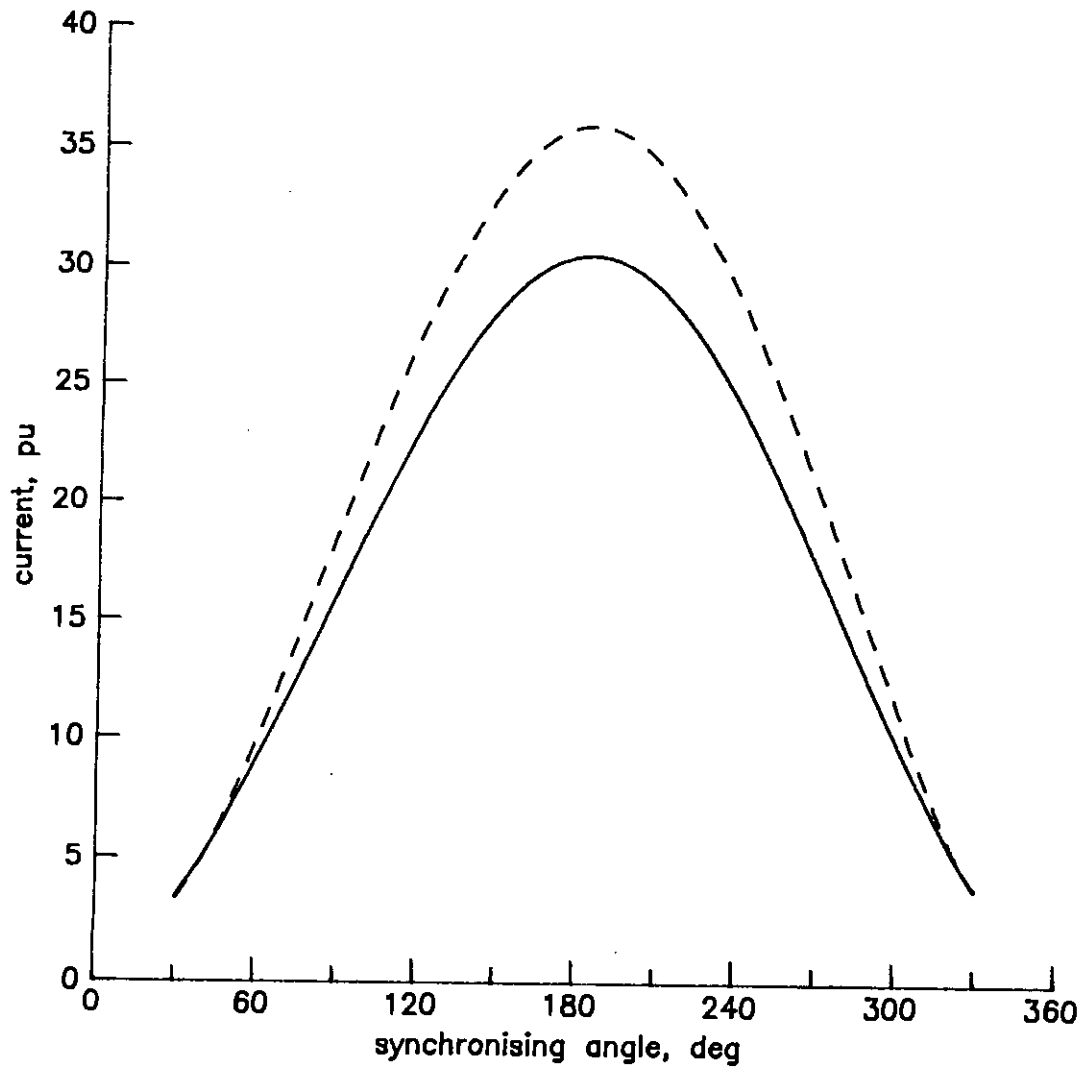


Fig 4.3 : Effect of saturation on maximum stator current following out of phase synchronisation of machine 'A'.

- - - with saturation
 ——— without saturation

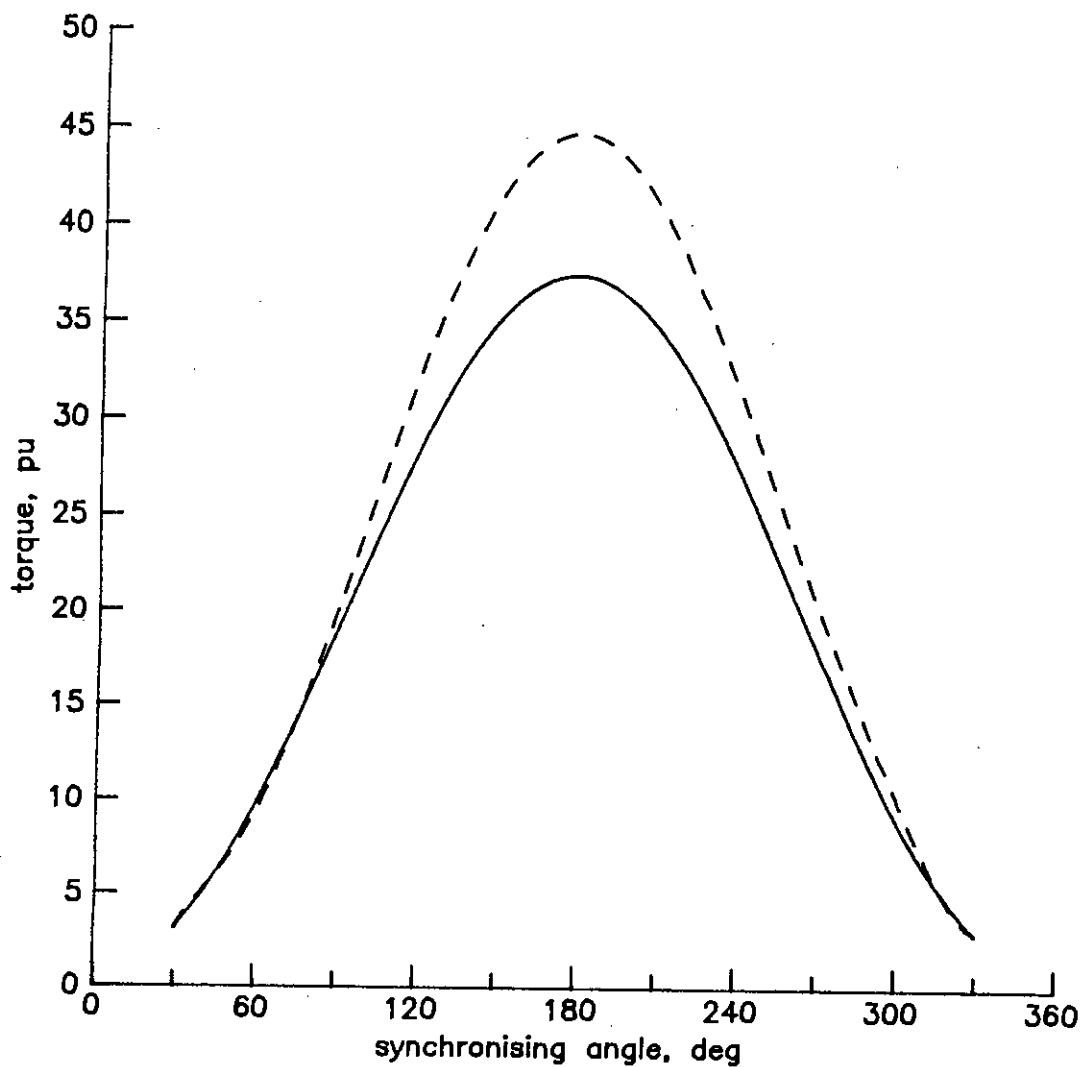


Fig 4.4 : Effect of saturation on peak to peak airgap torque following out of phase synchronisation of machine 'A'.

--- with saturation
 — without saturation

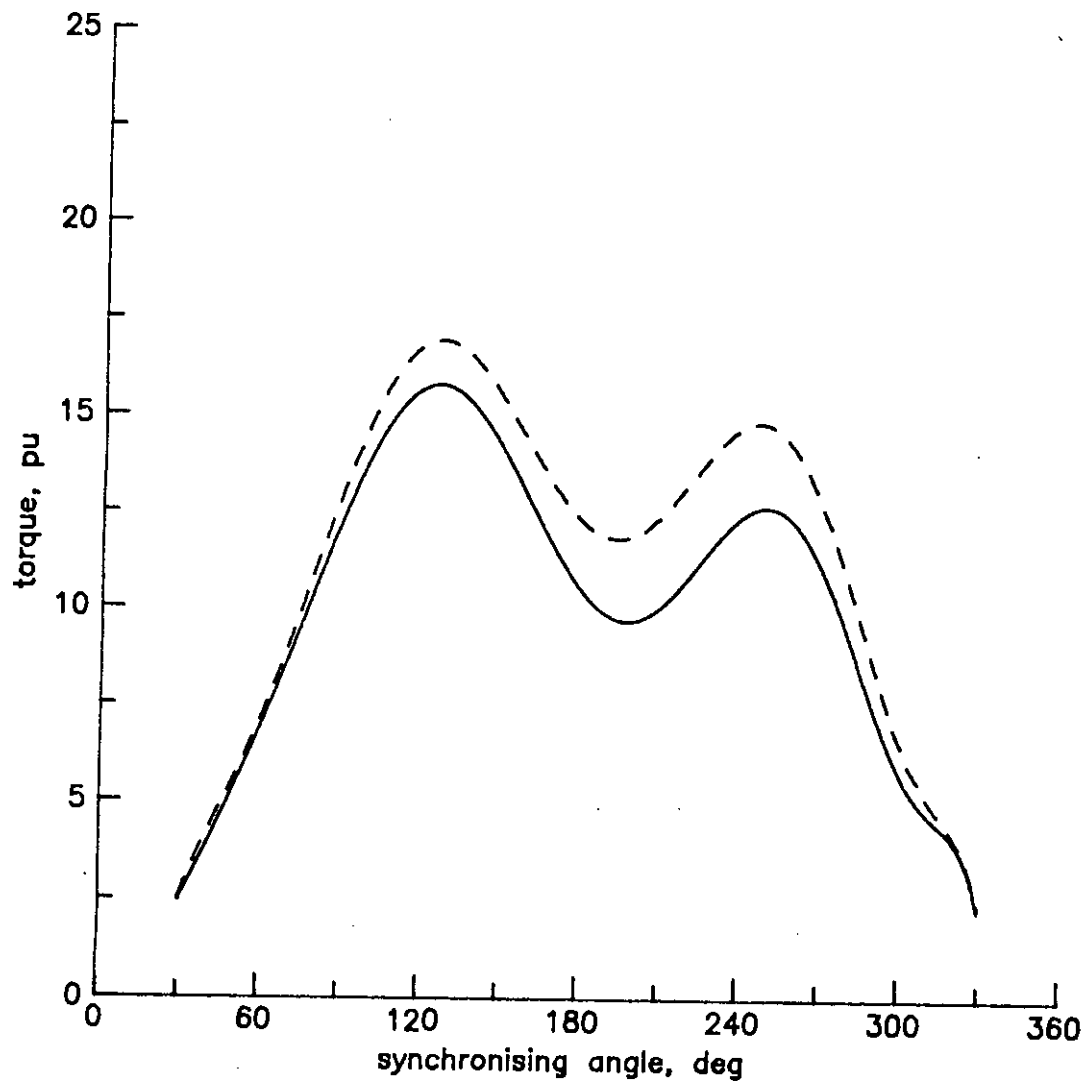


Fig 4.5 : Effect of saturation on peak to peak quill shaft torque following out of phase synchronisation of machine 'A'.

- - - with saturation
 ——— without saturation

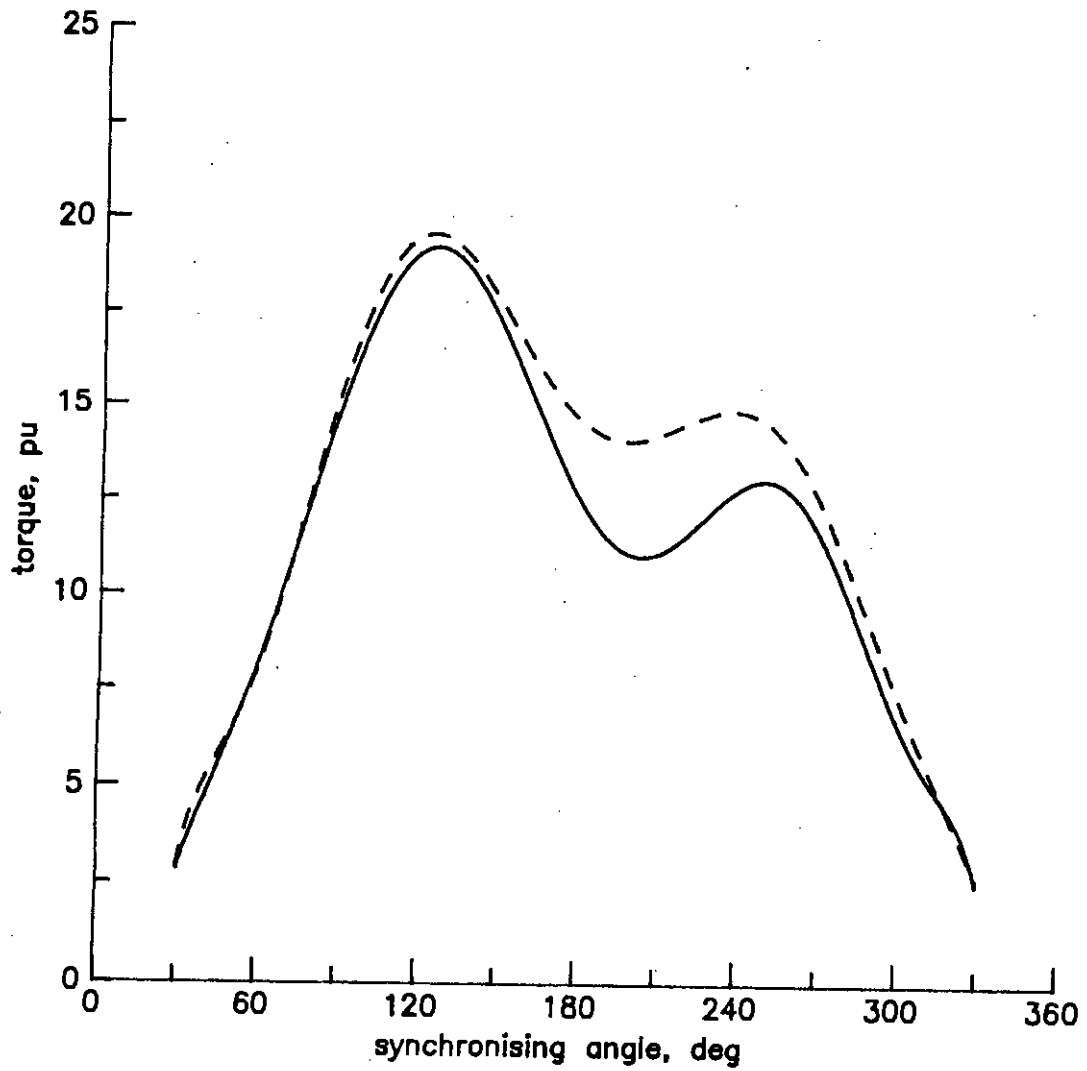


Fig 4-6 : Effect of saturation on peak to peak coupling shaft torque following out of phase synchronisation of machine 'A'.

--- with saturation
 ——— without saturation

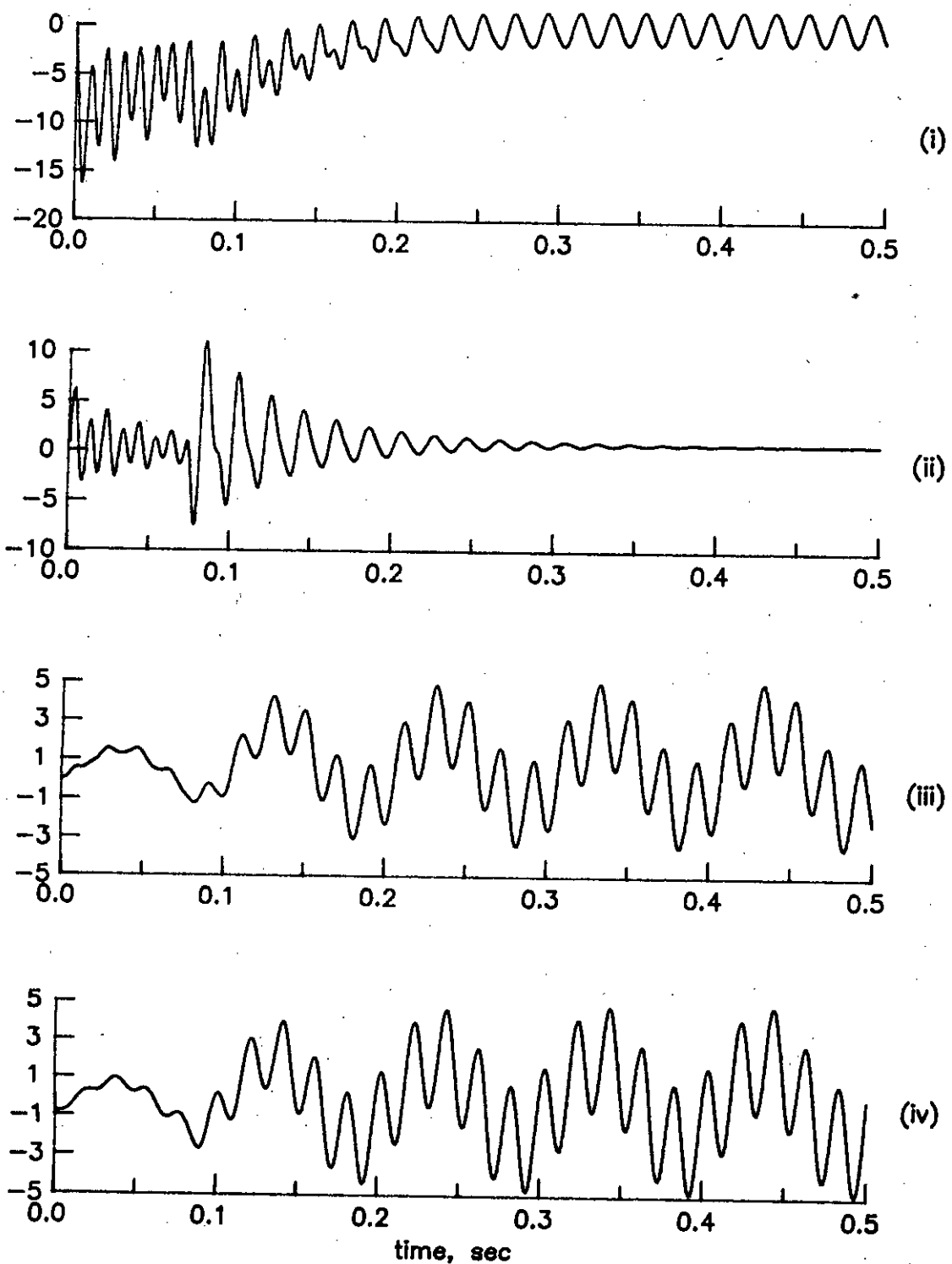


Fig 5.1 : Simulation of a fault throwing test on machine 'A'.
 $P=0.80$ pu $V=1.0147$ pu $I=0.8694$ pu

(i) stator current, pu (iii) quill shaft torque, pu
(ii) airgap torque, pu (iv) coupling shaft torque, pu

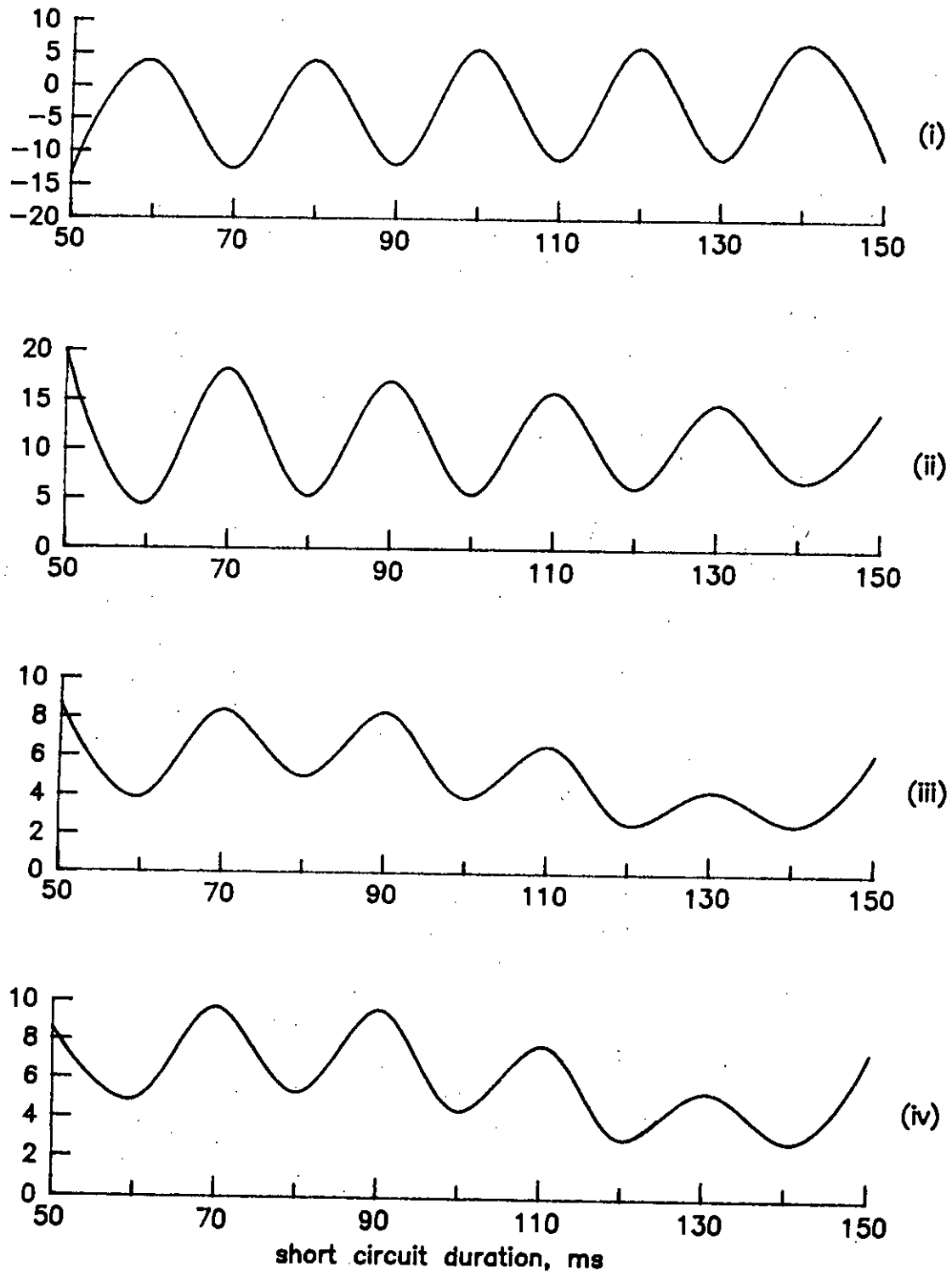


Fig 5.2 : Effect of fault duration on peak values during fault throwing test.

(i) stator current, pu (ii) airgap torque, pu
 (iii) quill shaft torque, pu (iv) coupling shaft torque, pu

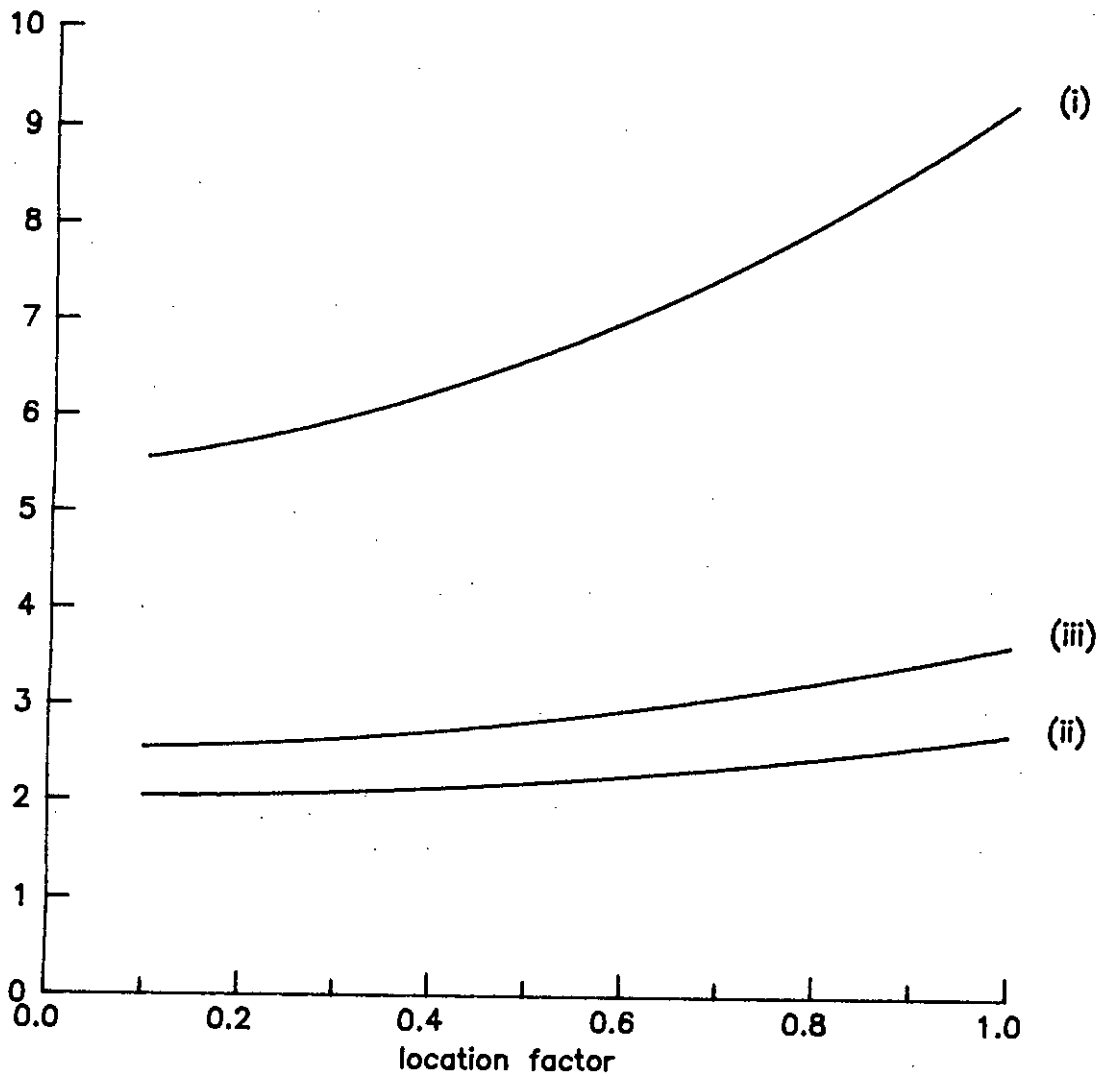


Fig 5.3 : Effect of fault location on peak to peak torques during short circuit period.

(i) airgap torque, pu (ii) quill shaft torque, pu
 (iii) coupling shaft torque, pu

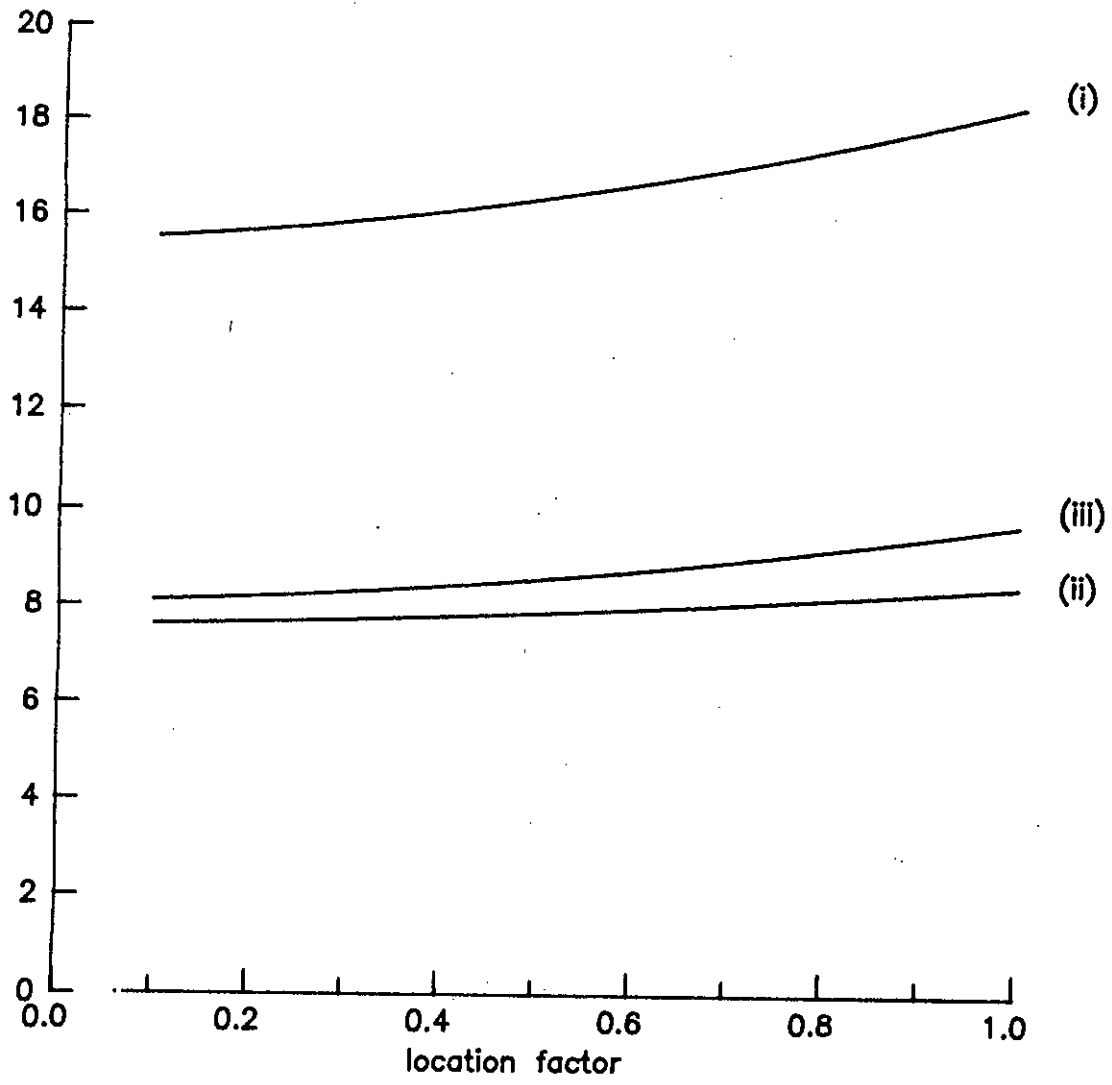


Fig 5.4 : Effect of fault location on peak to peak torques after fault clearance.

(i) airgap torque, pu (ii) quill shaft torque, pu
 (iii) coupling shaft torque, pu

